

MOLECULAR CLOUDS AND STAR FORMATION

Thesis by
Anneila Isabel Sargent

In Partial Fulfillment of the Requirements
for the Degree of
Doctor of Philosophy

California Institute of Technology
Pasadena, California

1978

(Submitted October 14, 1977)

ACKNOWLEDGEMENTS

My days as a graduate student have spanned such a large number of years that it is impossible to thank individually all the advisors, office-mates, fellow students and other friends who have, over that time, contributed in one way or another to my education.

I am very grateful to my current advisor, Peter Goldreich, for encouraging me to begin the research which constitutes this thesis and for his support throughout the last three years. Much of my enthusiasm to embark upon this course was inspired by a long collaboration with Jesse Greenstein, and, during the last months, the fruitful conclusion of that collaboration was often my sole reason for believing the present work would ever be finished. I am indebted to Gerry Neugebauer for detailed and constructive criticisms of drafts of both chapters, as well as for his advice on a number of troubled occasions.

It is a pleasure to thank Jill Knapp for introducing me to the technicalities of millimeter radio astronomy, for assisting with the early observations and for providing the initial 2 mm formaldehyde data. Robert Loren and Neal Evans, of the University of Texas at Austin, kindly obtained the 2 cm formaldehyde observations. I also appreciate use of the latter's models to derive densities from the formaldehyde measures. Unpublished ANS data were drawn to my attention by Reinder van Duinen. I am grateful to him both

(iii)

for these and for a number of helpful discussions.

A great deal of telescope time was necessary to this project and I appreciate the generous spans allocated to me at the Aerospace Corporation by Eugene Epstein. Observing time at the Millimeter Wave Observatory and the National Radio Astronomy Observatory is also gratefully acknowledged.

At various stages of this work I have had useful discussions with, or been assisted by, a number of people other than those mentioned above. In this context I should like to thank Charles Alcock, Steve Beckwith, Todd Boroson, Menachem Cimerman, Bob Dickman, Jay Elias, John Huchra, Frank Israel, Daniel Kunth, Fred Lo, Jon Romney, Ron Snell, Paul Vanden Bout, Julie White and Bill Wilson. I am also exceedingly grateful to Catherine Cesarsky, Althea Wilkinson and Anna Zytchow for sustaining my morale.

Chapter 1 was ably and obligingly typed by Helen Holloway. The remaining typing was done by Marilynne Rice under circumstances which leave me forever in her debt.

The long-suffering encouragement of my husband Wal, and the toleration of my daughters Lindsay and Alison has considerably eased the completion of this work. I cannot adequately express my indebtedness to them.

Throughout my graduate studies I was supported by a Graduate Research Assistantship funded by NSF Grant

MPS-72-05045 A02.

ABSTRACT

Observations of the $J = 1 \rightarrow 0$ transition of ^{12}CO were made in and around the region occupied by the young OB association Cepheus OB3 to determine the connection between newly formed stars and molecular clouds. An extended (20 pc x 60 pc) molecular cloud was detected and mapped, and additional observations of ^{13}CO and H_2CO were made at selected positions. The total mass of the cloud is $5 \times 10^3 M_{\odot}$. A range of velocities is seen over the cloud complex. This is comparable with the stellar velocities in the association.

Within the molecular cloud are found three regions in which different stages of star formation are identified. In one an embedded star may be present. Another appears to be collapsing on a time scale of $\sim 3 \times 10^5$ years to form a new subgroup of the OB association. The mass of this region, $500 M_{\odot}$, is sufficient to produce only the number of O and B stars typically found in association subgroups, suggesting that lower mass stars must form under different conditions. The third displays signs of enhanced density and is probably the precursor of a star forming region. All three regions are situated in that part of the molecular cloud which is closest to the association stars.

The membership and ages of the subgroups of the Cepheus OB3 association have been re-examined, and their

places of origin determined. Ages of $1-3 \times 10^5$ years and $5-7 \times 10^5$ years are found for younger and older subgroups respectively. Their birthplaces are not coincident but are situated at that end of the cloud where star formation still appears to be taking place. The younger subgroup appears to have formed closer to the active regions than did the older subgroup, so that there is a well-defined age sequence across the association which continues into the cloud.

There is currently little direct interaction between the stars and the molecular cloud, although a few younger subgroup stars still lie close to or within the complex. The absence of primeval gas in the environs of the older subgroup is attributed to the unusually high velocity of separation between these stars and the cloud.

It appears that the younger and still-forming subgroups of Cepheus OB3 are created in a different way from the older subgroup. However, the way in which star formation is initiated in this association remains uncertain.

TABLE OF CONTENTS

	Introduction	1
Chapter 1	Observations of the Cepheus Molecular Cloud	2
	I. Introduction	3
	II. Observational Selection	4
	III. CO Observations	6
	IV. Formaldehyde Observations	13
	V. Results	14
	VI. Detailed Studies of Cep-A, Cep-B, Cep-C	27
	VII. Summary	45
	References	48
Chapter 2	Star Formation in Cepheus OB3	50
	I. Introduction	51
	II. The Molecular Cloud	52
	III. The Cepheus OB3 Stars	77
	IV. The Present Relationship between the Molecular Cloud and the OB Association	103
	V. Star Formation in Cepheus OB3	109
	VI. Summary	119
	References	121

I. INTRODUCTION

This thesis contains two papers concerning the formation of stars in molecular clouds. A study has been made of the properties of the young OB association Cepheus OB3 and its related molecular cloud complex, with the intention of establishing how the association was created and how the cloud has subsequently evolved.

Detection and measurements of the molecular cloud are described in Chapter 1. Occasional references are made to following papers. These remarks may appear out of place in the context of the thesis, but result from the fact that this chapter is the first paper of a series on molecular clouds and star formation.

In Chapter 2 the observations of the Cepheus molecular cloud are analyzed, and the properties of the association stars are examined in detail. Finally, the results for the molecular cloud and the stars are combined to determine how star formation was initiated and how it may proceed in this particular case.

CHAPTER 1

OBSERVATIONS OF THE CEPHEUS OB3 MOLECULAR CLOUD

I. INTRODUCTION

It is well established that newly formed stars are frequently found in association with dense molecular clouds. Among the better known examples are the infrared cluster in Orion (Becklin, Neugebauer, and Wynn-Williams 1973; Liszt et al. 1974); the infrared sources and water maser found at the edge of the M17 cloud (Lada 1976; Elmegreen and Lada 1977); the compact H II regions, H₂O and OH masers and infrared sources located along the boundary of the molecular cloud connected with W3 (Mezger and Wink 1975; Harris and Wynn-Williams 1976), and the infrared objects, compact H II regions, H₂O and OH masers found in the region of the Mon R2 cloud (Downes et al. 1975; Kutner and Tucker 1975; Beckwith et al. 1976).

However, the way in which stars form within these clouds and the subsequent behavior of the clouds themselves is not well understood. In particular, if it is assumed that all molecular clouds collapse gravitationally to form stars, the resulting star formation rate is much greater than that observed (cf. Zuckerman and Palmer 1974). For the predicted and observed rates to agree, it is necessary that either contraction takes place on a time scale longer than that for free-fall collapse or that only a fraction of the cloud material forms stars.

To elucidate the relationship between star formation and molecular clouds, a detailed analysis of some group of newly formed stars and a related molecular cloud is required. To this end, two such groups, Cepheus OB3 and Perseus OB2, were selected, and associated molecular clouds were searched for, detected and mapped in the 115 GHz line of carbon monoxide. Sizes and masses of the clouds were determined from measurements of both the ^{12}CO and ^{13}CO lines, while their structure was investigated through the variation with position of line widths, temperatures and velocities.

In view of the abundance of available data and the extensive molecular observations involved in the current study, this paper will confine itself to a presentation of the observations of Cepheus OB3 only. A detailed interpretation of these data will be carried out in Chapter 2.

II. OBSERVATIONAL SELECTION

The young OB association Cepheus OB3 was selected primarily because it is young enough to be a site of recent star formation (its youngest stars are of age $\sim 4 \times 10^6$ years, comparable to the youngest optically visible stars in Orion OB1), but is also sufficiently old that its primeval cloud must have evolved to some extent. Its basic properties are described in Blaauw's (1964) list of O associations in the

solar neighborhood.

Cepheus OB3 is composed of two subgroups (cf. Fig. 1) of stars, the older being of age 8×10^6 years and the younger 4×10^6 years. This typical age difference between individual subgroups of an OB association suggests that there will be indications within any adjacent clouds of the beginnings of yet another epoch of stellar birth. At 730 pc the association is sufficiently close that the detection and measurement of infrared sources, molecular peaks and other signposts of protostars is facilitated.

The difference between the masses of OB associations ($\sim \text{few} \times 10^3 M_{\odot}$) and typical molecular clouds ($\sim 10^4 - 10^5 M_{\odot}$) can be explained if only a fraction of the cloud material forms stars. Thus analysis of the structure of a molecular cloud after some star formation has taken place may indicate the subsequent behavior of the cloud material and in particular whether or not it eventually disperses. Blaauw noted, and it is clear from inspection of the Palomar Sky Atlas, that the degree to which interstellar matter permeates OB associations decreases with association age. As might be expected, a considerable amount of interstellar material is still present in the vicinity of Cepheus OB3 so that the region is particularly suitable for studying this question of cloud evolution.

This association has the further advantage that the

properties of its stars have already been investigated in some detail. Proper motions, association membership and radial velocities of the stars, as well as expansion velocities of the two subgroups in Cepheus OB3 have been determined by Garmany (1973). Spectral classes on the MK system were assigned by Garrison (1970) in the course of an investigation of total to selective absorption across the association. The stars have been well-studied photometrically, from the original UBV measurements of Blaauw, Hiltner and Johnson (1959), through the ubvy and $H\beta$ photometry of Crawford and Barnes (1970), to the ultraviolet observations of the ANS instrument (Kester 1977). In addition, an area of considerable extent ($l = 90^\circ$ to 115° , $b = -1^\circ$ to $+15^\circ$) around and including Cepheus OB3 was surveyed in the 21-cm line of neutral hydrogen by Simonson and van Someren Greve (1976). They derived a possible model of the OB association with respect to the surrounding neutral hydrogen. Finally, to augment this already large pool of data, a search has been made by Harris (1976), in conjunction with the observations described here, for compact H II regions in the neighborhood of S155, the H II region located in the southwest of Cepheus OB3.

III. CO OBSERVATIONS

The 4.6 meter telescope of the Aerospace Corporation in

El Segundo, California was used to map a $1.5^\circ \times 4.5^\circ$ area of Cepheus in the $J = 1 \rightarrow 0$ transitions of ^{12}CO (115 GHz) and ^{13}CO (110 GHz). The telescope has a main beam efficiency of 70% and a half-power beam width 2.5 arcminutes. Most observations were obtained between 1975 December and 1976 March when weather conditions were excellent with zenith optical depths of ~ 0.3 at 115 GHz and ~ 0.2 at 110 GHz. Typical integration times of 10 minutes for ^{12}CO and 15 minutes for ^{13}CO were used. The single sideband system temperature at CO frequencies using an uncooled mixer receiver was ~ 1200 K. Spectral lines were detected with a 64 channel filter bank giving a resolution of 250 kHz (0.65 km s^{-1} at 115 GHz) per channel. Baseline stability was achieved by frequency switching with 8 MHz separation between signal and reference bands. The reference line was inverted with respect to the signal and later folded with it, thereby effectively increasing the integration time. The corrected antenna temperature, T_A^* , is the temperature measured by a lossless antenna above the earth's atmosphere, where

$$T_A^* = \frac{h\nu}{k} [F(T_B) - F(T_{bb})] ,$$

and

$$F(T) = \left[\exp\left(\frac{h\nu}{kT}\right) - 1 \right]^{-1} .$$

T_B is the source brightness temperature and T_{bb} is the temperature of the microwave background. To determine T_A^*

the signal observed on source is corrected for atmospheric attenuation by multiplying by a factor of $e^{\tau_0 \sec z}$, where z is the zenith distance of the source observed and τ_0 is the zenith optical depth. Measurements of τ_0 by tipping were made every three to four hours during each observing session. This corrected signal is scaled to the system temperature using an observing chopper at 300 K which rotated in the field of view of the feed horn. As a further check on the stability of the system Orion A was observed each day and one point of relatively strong CO emission within the cloud was monitored each hour throughout all observing runs. The final values of T_A^* are on a scale such that for Orion A T_A^* (^{12}CO) = 70 K and T_A^* (^{13}CO) = 10.9 K.

a) ^{12}CO

Observations of ^{12}CO were first made at spacings of ten arcminutes (i.e., four beam widths) in right ascension and declination. Mapping was continued until the boundaries of the cloud (defined at $T_A^* \leq 2.5$ K) could be specified.

A primary concern of the survey was to detect small scale structure in the clouds and, in particular, to determine the location of possible sites of star formation. Since lines exhibiting enhanced temperatures, wide wings or a considerable degree of broadening are indicators of such sites, more detailed measurements at spacings of two

arcminutes in right ascension and declination were made about any profile which displayed these properties. The usual criterion for use of this finer grid was that $T_A^* \geq 10$ K. This criterion incidentally selected regions displaying broadened or wide-winged lines for finer grid measures.

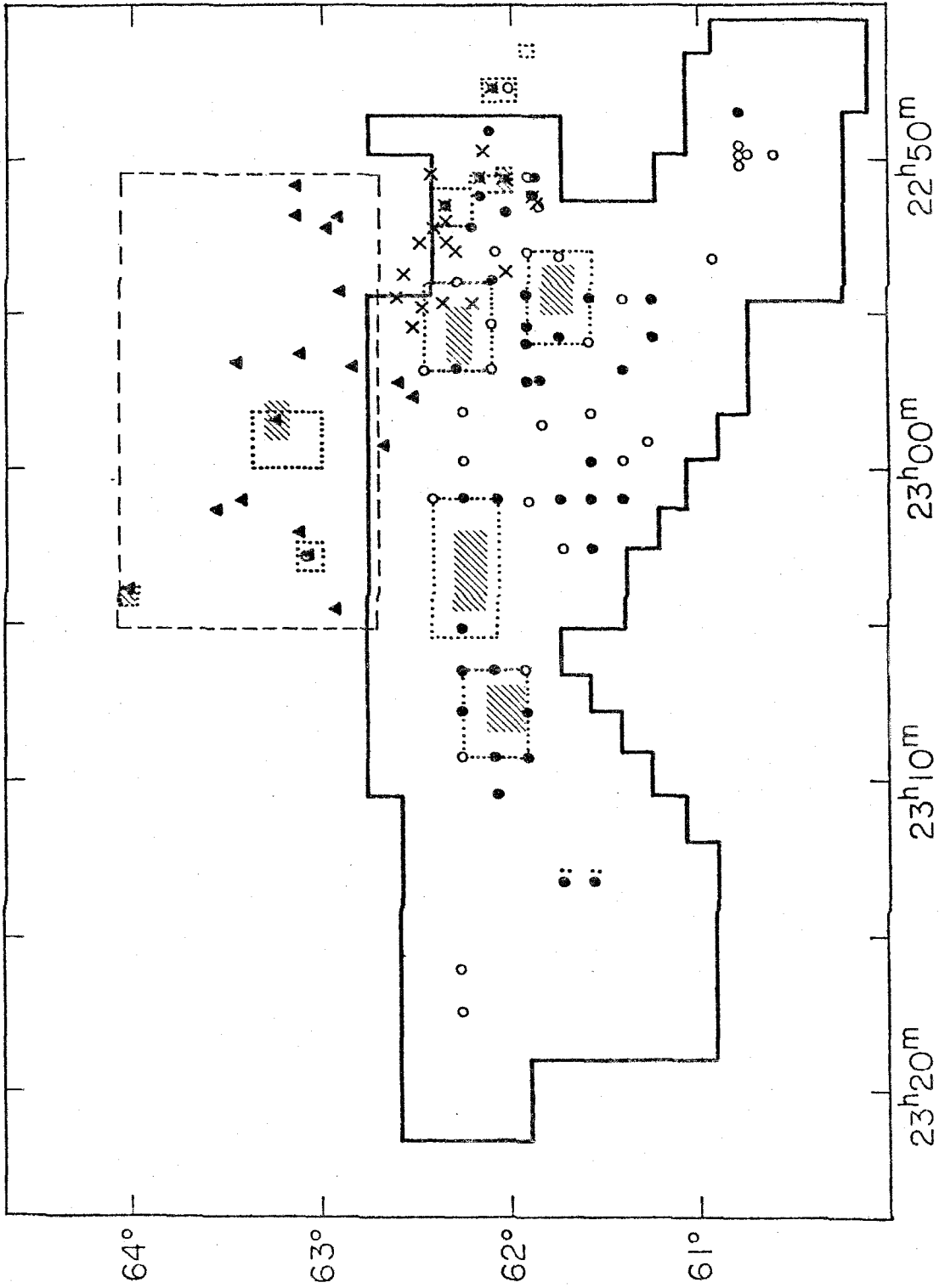
Observations were also made in the directions of the OB association members. Mapping was carried out around a few of the younger subgroup stars, several of which lie within the cloud boundaries. Gas was unambiguously detected in the direction of only one older subgroup member. In a few doubtful cases measurements were made as indicated in Figure 1. As a further check for the presence of CO outside the primary cloud boundaries, but in the general vicinity of the association stars, observations at 20 arcminute spacings were made along the length of the cloud and perpendicular to it beyond the declination of the most northerly association member. The area encompassed by these observations is shown in Figure 1.

b) ^{13}CO

Observations of the rarer isotope were for the most part confined to the vicinity of the "hot spots" as determined by the ^{12}CO survey. Other detailed measurements were made (see Fig. 1) in the neighborhood of the association stars 11, 56, and 75. The numbering system adopted is that of Blaauw,

FIGURE 1

Areas of the sky covered by observations at various separations. A heavy solid line outlines the region where ^{12}CO measurements at 10' spacings were made; 2' and 20' sampled areas are bounded by dotted and dashed lines respectively. Measurements of ^{13}CO at 2' spacings were made over the hatched zones. Other ^{13}CO observations are indicated by filled circles where the isotope was detected and by open circles where it was absent. The stars of the association are represented by crosses and filled triangles, crosses denoting members of the younger subgroup, and filled triangles members of the older subgroup of Cepheus OB3.



8 (1950)

α (1950)

Hiltner and Johnson (1959). An effort was made to continue observations of the hot spots outwards from a central position until $T_A^*(^{13}\text{CO}) \leq 1$ K. In some directions further observations were made at distances of ten arcminutes from the central position in the hope of estimating the extent of the presence of ^{13}CO . The results will be discussed in § Vb. Figure 1 illustrates how far this procedure was employed. Further ^{13}CO observations were made where broadened or multiple lines were seen in ^{12}CO . In cases where the ^{13}CO line was detected to be ≥ 3 K some large scale mapping was carried out.

c) High Resolution Measurements

Observations at higher spatial resolution are needed to clarify the nature of hot spots found in the initial Aerospace survey. These hot spots were therefore studied at ^{12}CO and ^{13}CO frequencies using the 11-meter telescope of the National Radio Astronomy Observatory at Kitt Peak, Arizona¹ in conjunction with the 256 × 250 kHz filter banks.

¹The National Radio Astronomy Observatory is operated by Associated Universities for Research in Astronomy, Inc., under contract with the National Science Foundation.

The single side-band system temperature was ~ 1000 K while the half-power beam-width is ~ 65 arcseconds at 115 GHz. Similar calibration procedures to those at Aerospace were employed. Values of T_A^* are on a scale such that for Orion

A $T_A^*(^{12}\text{CO}) = 60 \text{ K}$ (Ulich and Haas 1976). The telescope was operated in the position switching mode. Off-source positions were typically 30 arcminutes away from the source, at locations previously determined to be free of CO emission. Useful, high resolution profiles were obtained, but detailed measurements about the positions of peak T_A^* are very limited. Both with respect to line shape and to peak T_A^* observed these profiles are in excellent agreement with those obtained in the same directions but at lower resolution at Aerospace.

IV. FORMALDEHYDE OBSERVATIONS

Since the presence of the $J_{K-K+} = 2_{12} \rightarrow 1_{11}$ transition of formaldehyde is often associated with relatively high molecular hydrogen densities ($n_{\text{H}_2} = 10^4 - 10^5 \text{ cm}^{-3}$) (Lucas, Encrenaz and Falgarone 1976 and references therein), a search was made at and around the positions of the hot spots for this 140 GHz line. The observations were made in 1976 March and 1976 May with the 5-meter telescope of the Millimeter Wave Observatory, Fort Davis, Texas² operated in a

²The Millimeter Wave Observatory is operated by the Electrical Engineering Research Laboratory of the University of Texas at Austin.

frequency switching mode. The single side-band system temperature for H_2CO was 2400 K, and the half-power beamwidth 2 arcminutes. The spectral resolution was 0.53 km s^{-1} .

Calibration was carried out by the usual chopper wheel technique. Orion A, with $T_A^*(\text{H}_2\text{CO}) = 4.8 \text{ K}$, was observed daily to establish a standard comparison. Measurements were made at spacings of 2 arcminutes around the positions of peak intensity to determine the sizes of the H_2CO emission regions.

V. RESULTS

a) $\text{^{12}CO}$

The velocity at which peak antenna temperature, $T_A^*(\text{^{12}CO})$ occurs is not the same throughout the cloud, but ranges from -5 km s^{-1} to -15 km s^{-1} ; the peak emission appears most frequently at velocities around -10 km s^{-1} . In Figure 2 are shown contours of peak $T_A^*(\text{^{12}CO})$ within this velocity range. The elongation of the molecular cloud parallel to the galactic plane is particularly marked. Positions of the association stars with respect to the cloud are also displayed in this figure, the older subgroup being represented by filled triangles and the younger by crosses. To facilitate later discussion, regions of the cloud which will be referred to individually have been designated A, B, C, etc., in the figure. In Figure 3 the contours of $T_A^*(\text{^{12}CO})$ as shown in Figure 2 are superimposed on the Palomar Sky Survey print of the Cepheus region. The contours of Cep-B partially obscure S155.

FIGURE 2

Contours of peak antenna temperatures, T_A^* (^{12}CO). As in Figure 1 the crosses and triangles symbolize the association stars. Areas Cep-A, -B, -C, -D, -E, and -F discussed in the text are indicated. At Cep-A and -B the undesignated contours represent values of T_A^* increasing from 10 K to 25 K by increments of 5 K.

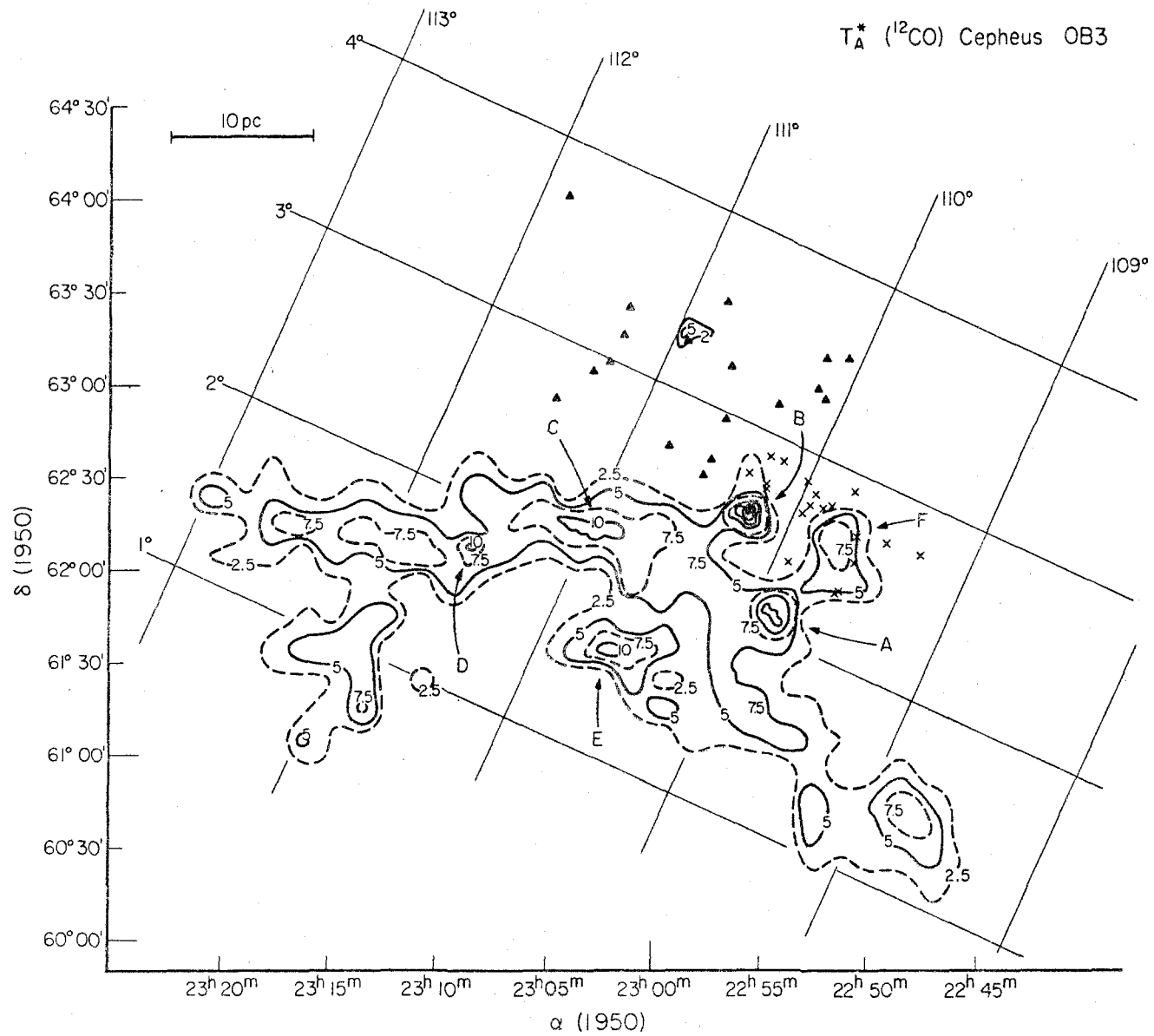
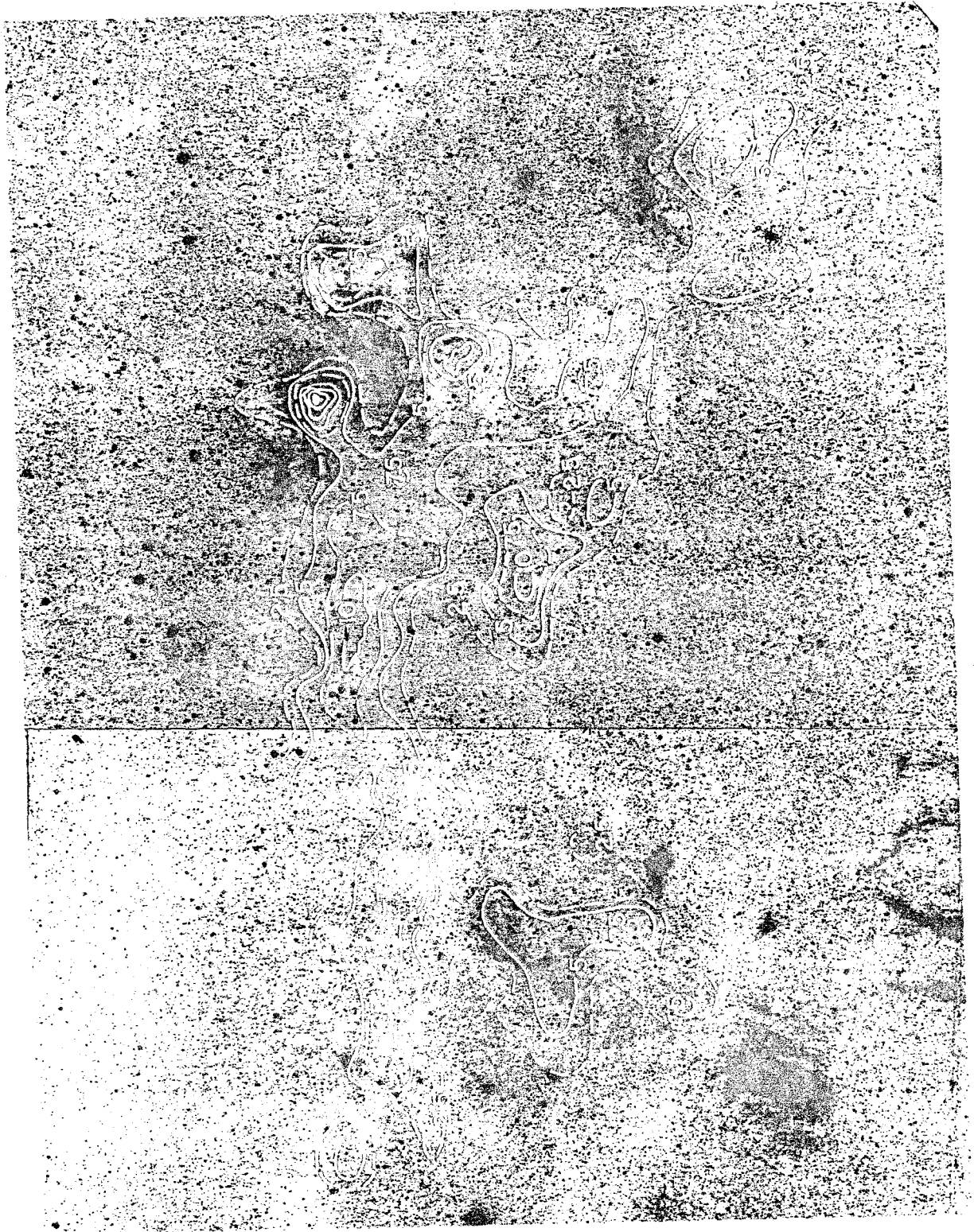


FIGURE 3

Contours of peak antenna temperature, $T_A^*(^{12}\text{CO})$, for the Cepheus cloud superimposed on the Palomar Sky Survey print of the region. The orientation of the cloud with respect to equatorial and galactic coordinates is as shown in Figure 2.



The maps of Cep-A, -B, -C, -D, and -E derived from higher positional sampling were found to be in good agreement with those determined from mapping at $10' \times 10'$ spacings. Limited $2' \times 2'$ mapping of Cep-F, however, indicates the presence of small scale structure not shown in Figure 2. Several of the younger association members lie within the boundaries of Cep-F and it is possible that the differences between the results of the $10' \times 10'$ survey and the $2' \times 2'$ measures are attributable to the presence of these stars.

A few isolated observations around $\alpha = 22^{\text{h}}47^{\text{m}}$, $\delta = 62^{\circ}00'$ (cf. Fig. 1) near an association star reveal the presence of CO at a velocity appropriate to the primary cloud. From examination of the PSS print and the available measurements, it seems likely that this secondary component is fairly small, perhaps comparable to Cep-B in size. The highest values of $T_A^*(^{12}\text{CO})$ noted are of the order of 10 K. Further mapping of this zone and of Cep-F is clearly important.

Across large areas of the Cepheus cloud double, and frequently triple, features are visible in the ^{12}CO profiles. Maps of T_A^* at a number of velocities between -5 km s^{-1} and -12 km s^{-1} were therefore constructed and are displayed in Figures 4a through 4e. The T_A^* plotted is the highest value of that quantity noted within $\pm 0.65 \text{ km s}^{-1}$ of the velocity quoted for each map. For comparison Figure 2 is redrawn to

FIGURE 4a

Contours of $T_A^*(^{12}\text{CO})$ at $V_{\text{LSR}} = -12.0 \text{ km s}^{-1}$.

FIGURE 4b

Contours of $T_A^*(^{12}\text{CO})$ at $V_{\text{LSR}} = -10.7 \text{ km s}^{-1}$.

FIGURE 4c

Contours of $T_A^*(^{12}\text{CO})$ at $V_{\text{LSR}} = -9.4 \text{ km s}^{-1}$.

FIGURE 4d

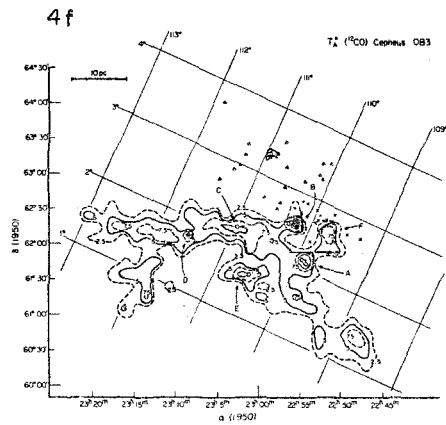
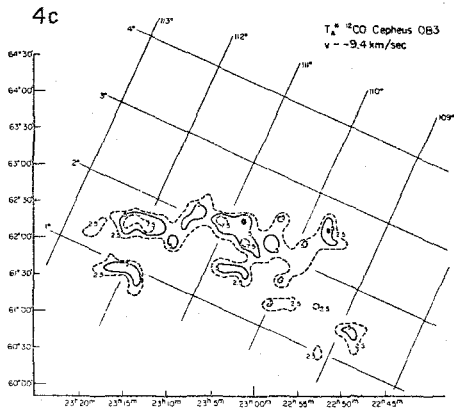
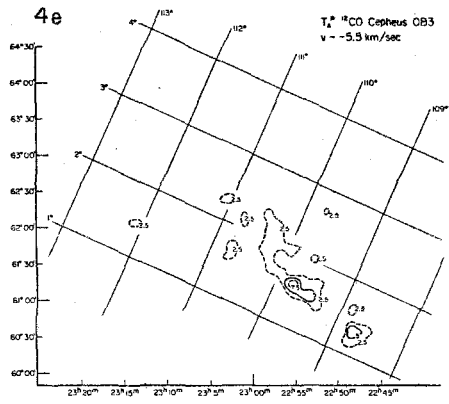
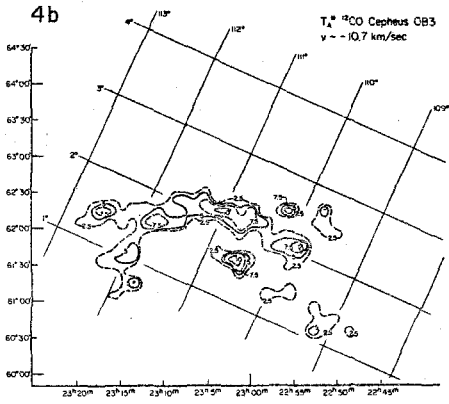
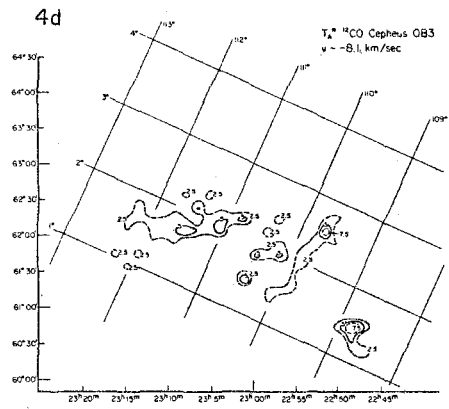
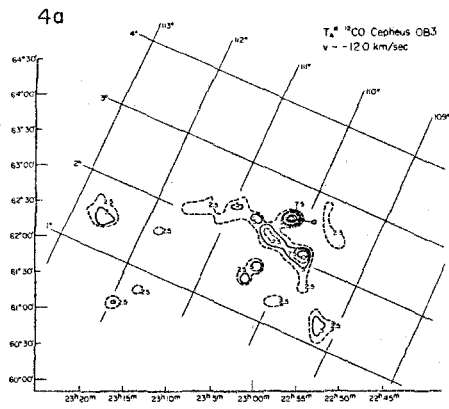
Contours of $T_A^*(^{12}\text{CO})$ at $V_{\text{LSR}} = -8.1 \text{ km s}^{-1}$.

FIGURE 4e

Contours of $T_A^*(^{12}\text{CO})$ at $V_{\text{LSR}} = -5.5 \text{ km s}^{-1}$.

FIGURE 4f

Figure 2 reproduced on same scale as Figures 4.



the same scale alongside these figures. Maps were not produced at $V_{\text{LSR}} \sim -7 \text{ km s}^{-1}$ or $V_{\text{LSR}} < -12 \text{ km s}^{-1}$ where peaks in T_{A}^* occur only rarely. Evidently the cloud comprises a number of components at different velocities, each of which follows to some degree the overall elongated pattern noted above.

It is evident from a comparison of Figures 4a through 4e and Figure 2 that the strongest emission from the region of the cloud closest to the association stars occurs at velocities near -12 km s^{-1} . The feature observed at this velocity falls off in intensity quite rapidly, to be replaced by emission closer to -10.7 km s^{-1} , particularly in the vicinity of Cep-A, Cep-C and Cep-E. Emission at more positive velocities tends on the whole to be patchily distributed, or at least seems uncorrelated with the positions of either the hot spots or the stars.

The range of cloud velocities observed here is well within the range of the association stellar velocities. The stars have values of V_{LSR} , measured with typical errors of $\pm 5 \text{ km s}^{-1}$, extending in value from 0 km s^{-1} to -30 km s^{-1} , with a mean of -11 km s^{-1} (Garmany 1973; see also Simonson and van Someren Greve 1976). For the eleven younger association members for which radial velocities are available, the mean is $\sim -15 \text{ km s}^{-1}$. The V_{LSR} of the H II region, S155, determined by Miller (1968) using the H α line on standard

slit spectrograms, and by Georgelin (1975) from photographic Fabry-Perot interferometry, is also -15 km s^{-1} . Errors quoted are typically $4-8 \text{ km s}^{-1}$. In view of the excellent agreement between results acquired by such widely differing techniques it is presumed that some confidence may be placed in the value -15 km s^{-1} . It is notable that in Cep-B, the region of the molecular cloud closest to S155, strong ^{12}CO emission occurs at a very similar velocity, -12 km s^{-1} .

Several of the younger association members lie in the direction of or close to Cep-F. As may be seen from Table 1 only stars 11 and 24 have radial velocities close to those at which emission is detected from the cloud. In the direction and at the velocity of both these stars the CO emission is decidedly weak (almost at the limit of detectability for 24) and quite localized. In general, emission from Cep-F occurs between -8 km s^{-1} and -9 km s^{-1} (cf. Figs. 4c and 4d), but close to stars 11 and 24 the line profiles are distorted toward more negative velocities, presumably as a result of contamination by gas associated with the stars. Occasionally CO was seen near to, but not precisely in the direction of, a stellar position. In these cases a designation in Table 1 such as "17-8S4E" indicates a position 8 arcminutes south and 4 arcminutes east of star 17.

With the exception of star 56 and possibly star 75 there is no evidence for the existence of CO in the direction

TABLE 1
 VELOCITIES OF CO EMISSION AT AND NEAR
 ASSOCIATION STARS

Position ¹	α (1950)	δ (1950)	$V_{\text{LSR}}(\text{star})^2$ km s ⁻¹	$V_{\text{LSR}}(\text{CO})$ km s ⁻¹
2-4S	22 47 42	+62 00 04	+ 1	-12
10-4E	22 51 08	+62 10 29	-23	-10
11	22 50 37	+62 02 50	-13	-11
15	22 51 18	+61 52 46	-29	- 9
16	22 51 33	+61 52 07	-22	-10
17-8S4E	22 52 11	+62 12 48	...	- 9
24	22 52 39	+62 20 44	-12	-12:
56	22 58 33	+63 14 52	-14	-14
75	23 03 56	+64 01 30	-13	-15:

¹Star numbers from Blaauw, Hiltner and Johnson (1959)

²Garmany (1973)

of older subgroup members of Cepheus OB3. Within the primary cloud emission at such negative velocities (cf. Table 1) is only observed close to the northwestern boundary.

To summarize, ^{12}CO emission at more negative velocities (i.e., $\leq -12 \text{ km s}^{-1}$) tends to be confined to the northern edges of the cloud around Cep-B, S155 and close to the association stars; in the regions of broadened lines (e.g. Cep-A, Cep-C) where future star formation might be expected to take place (cf. §§ VI and VII), peak T_A^* occurs at less negative velocities, between -10 km s^{-1} and -11 km s^{-1} ; emission at more positive velocities arises from what seem to be fairly tenuous extended regions in which there are as yet no indications of star formation.

b) ^{13}CO

In the Cepheus molecular cloud ^{13}CO was detected in Cep-A, -B, -C and -D and at the positions indicated by filled circles in Figure 1. Detailed contour maps of T_A^* (^{13}CO) for Cep-A, -B and -C are presented in the sections dealing specifically with these regions (cf. § VI). Observations at the locations of Cep-E and Cep-F imply that ^{13}CO is present to extents at least comparable with Cep-B.

Insufficient measurements are available to follow the velocity patterns as closely as in § Va. Moreover, the secondary features seen in ^{12}CO are rarely strong enough for equivalent ^{13}CO emission to be expected. Nevertheless, there

is excellent agreement throughout the cloud between the velocities at which maxima in $T_A^*(^{12}\text{CO})$ and $T_A^*(^{13}\text{CO})$ appear. Although multiple lines are not detected from the rarer isotope, at the positions where these are seen in ^{12}CO weak and broad ^{13}CO features, encompassing the velocities of the various ^{12}CO emission peaks, are observed.

The ^{12}CO observations did not justify searches for ^{13}CO at stellar positions other than those given in Table 1. Detections were made at and around the locations of stars 11, 15 and 56, although the extent, as expected, was much less than that of ^{12}CO . ^{13}CO was also found near stars 2, 10 and 17. The velocity of peak T_A^* is in all cases the same for both isotopic species.

The ^{13}CO data confirm the velocity structure implied by the ^{12}CO observations of the cloud complex and indicate the areas where density may be enhanced (cf. Chapter III). In portions of the cloud closest to the association stars and to S155 (e.g. Cep-B and Cep-F), measurements of the rarer isotope are neither as intense nor as extended as in Cep-A and Cep-C (cf. § VI), where particularly broad ^{12}CO lines are found. Interpretation of these profiles as increased density indicators will be discussed in detail in Chapter III.

c) H₂CO

Cep-A, -B and -C were examined for 140 GHz emission from H₂CO as described in § IV. At Cep-A and Cep-C 140 GHz H₂CO is unambiguously detected over areas approximately 6 arcminutes square, with maximum values of $T_A^*(\text{H}_2\text{CO}) \sim 0.9$ K and 0.6 K respectively. The velocities of peak $T_A^*(\text{H}_2\text{CO})$, being of the order of -10 km s^{-1} , are comparable with those of peak $T_A^*(^{12}\text{CO})$ and $T_A^*(^{13}\text{CO})$. It is doubtful if H₂CO is present at Cep-B. This result may be related to the fact that values of $T_A^*(^{13}\text{CO})$ observed there were considerably lower than those found at Cep-A and Cep-C.

VI. DETAILED STUDIES OF CEP-A, CEP-B, CEP-C

The regions Cep-A, -B and -C were observed at higher resolution in ¹²CO and examined for the presence of ¹³CO and H₂CO as described in §§ III and IV. Relevant parameters for each region are presented in Table 2.

a) Cepheus-A

Perhaps the most interesting portion of the Cepheus OB3 cloud complex is Cep-A. In Figure 5 are shown the ¹²CO and ¹³CO line profiles observed around the center of the zone. Over a small region these profiles are characterized by deep minima, possibly the result of self-absorption. The variation of this phenomenon with position is clearly illustrated. Note that the ¹²CO profiles were obtained with a different

TABLE 2

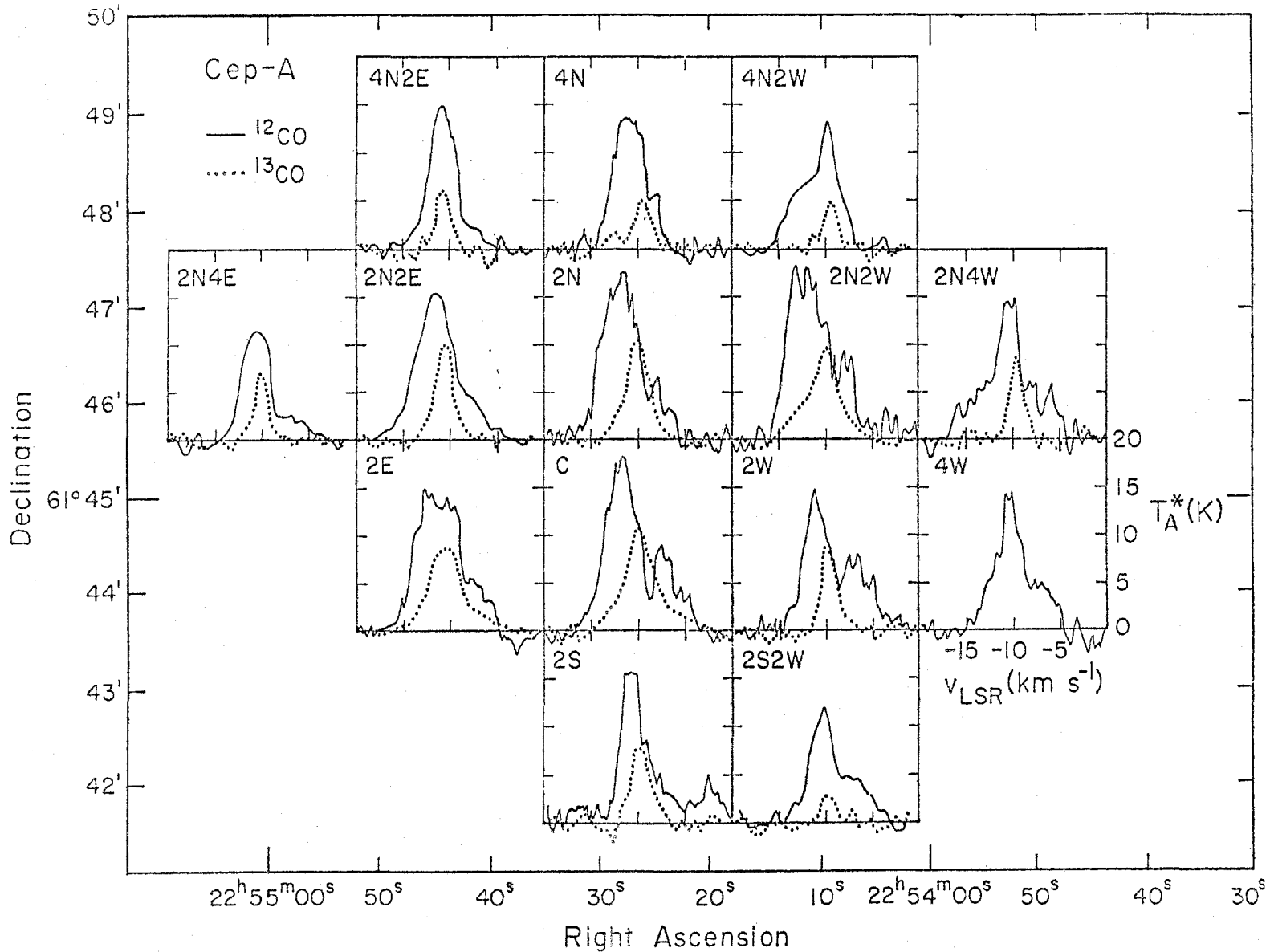
OBSERVATIONS OF INDIVIDUAL REGIONS IN THE CEPHEUS OB3 CLOUD

	α (1950)	δ (1950)	T_A^* (K)	V_{LSR}^{12CO} (km s ⁻¹)	T_A^* (K)	V_{LSR}^{13CO} (km s ⁻¹)
Cep-A	22 ^h 54 ^m 10 ^s	+61°44'36"	18:†	-12:†	11.0	-10.3
Cep-B	22 55 27	+62 18 37	29.0	-12.3	8.1	-12.3
Cep-C	23 03 38	+62 12 23	13.4	-10.3	9.1	-10.3

† Colon indicates approximate measurement

FIGURE 5

^{12}CO and ^{13}CO profiles observed about the central region of Cep-A. 2W, 2N, etc., refer to observations 2 arcminutes west of center, 2 arcminutes north of center and so on. The ^{12}CO profiles labeled 4N2E, 4N2W, 2N4E, 2N2E and 2S2W, as well as all ^{13}CO data, are from the Aerospace 5-m. Other ^{12}CO data are from the 11-m NRAO instrument.



instrument and at higher resolution than their ^{13}CO equivalents. Contours of $T_A^*(^{13}\text{CO})$ are displayed in Figure 6. Because interpretation of the ^{12}CO profiles is complicated by the absorption feature no equivalent contours of $T_A^*(^{12}\text{CO})$ are presented.

From Figure 5 it is evident that the absorption feature is present only in the immediate vicinity of the central position, with the ^{12}CO intensity minimum lying at -8.8 km s^{-1} and the ^{13}CO maximum at -10.3 km s^{-1} . Where the feature is absent, the ^{12}CO and ^{13}CO maxima appear at the latter velocity. Displacement to yet more negative velocities of the ^{12}CO maxima at positions north and east of center is attributable to the presence of an additional component at $\sim -12 \text{ km s}^{-1}$. The 2 mm H_2CO lines observed at Cep-A are shown in Figure 7. Usually the velocity of the H_2CO maximum is the same as that of the ^{13}CO peak at the same position, but a component at $\sim -12 \text{ km s}^{-1}$ is clearly present at the central position. Comparing Figures 5 and 7 it is clear that in Cep-A the presence of a ^{12}CO absorption feature is well correlated with the detection of 2-mm H_2CO .

b) Cepheus-B

The highest values of $T_A^*(^{12}\text{CO})$ in the Cepheus OB3 cloud are found in Cep-B. The position is marked by a cross in Figures 8a and 8b, where are shown contours of $T_A^*(^{12}\text{CO})$ and $T_A^*(^{13}\text{CO})$ respectively. Emission from Cep-B is primarily at

FIGURE 6

Contours of $T_A^*(^{13}\text{CO})$ at $V_{\text{LSR}} = -10.3 \text{ km s}^{-1}$ for Cep-A.

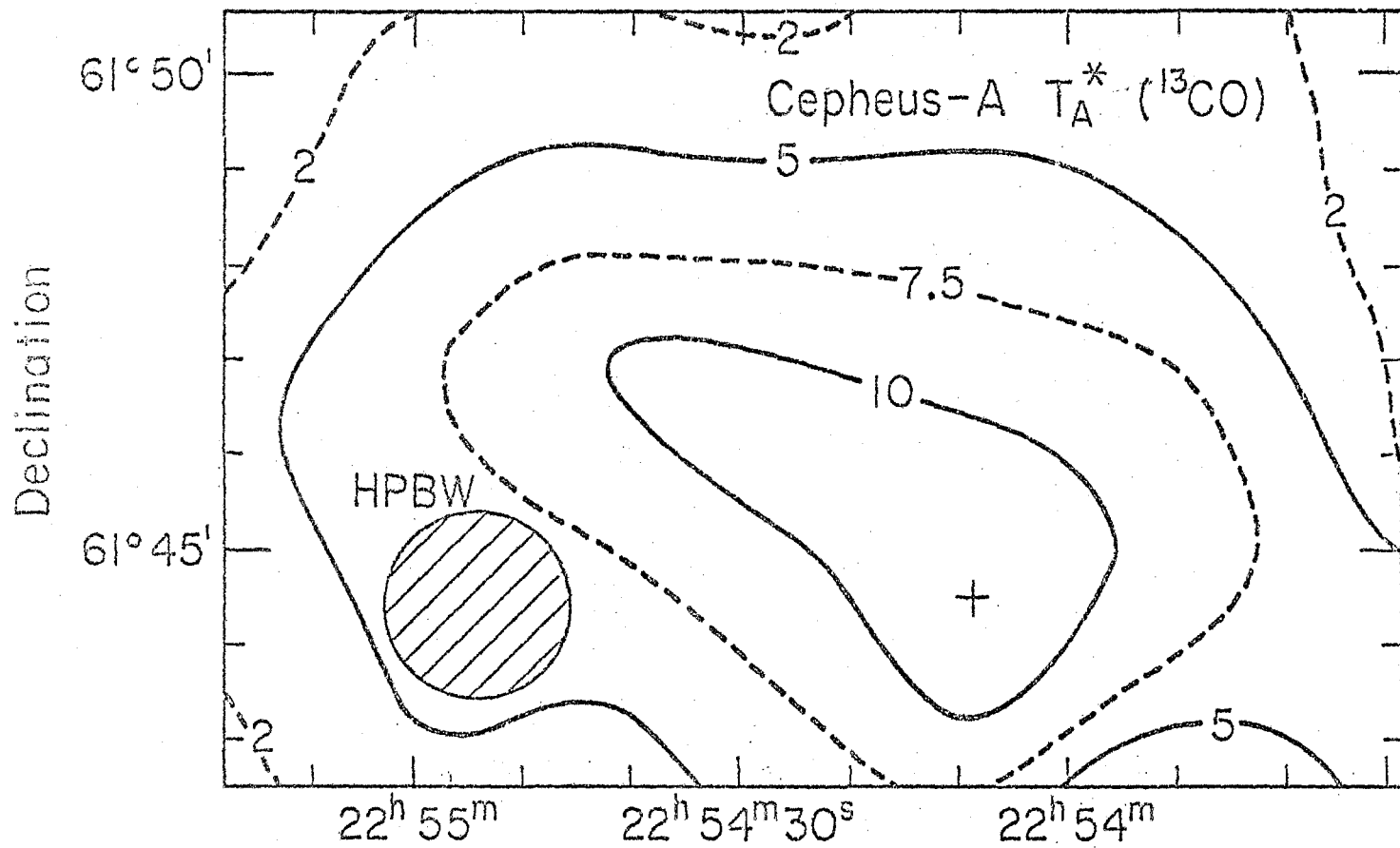


FIGURE 7

H₂CO profiles observed over the central region of
Cep-A.

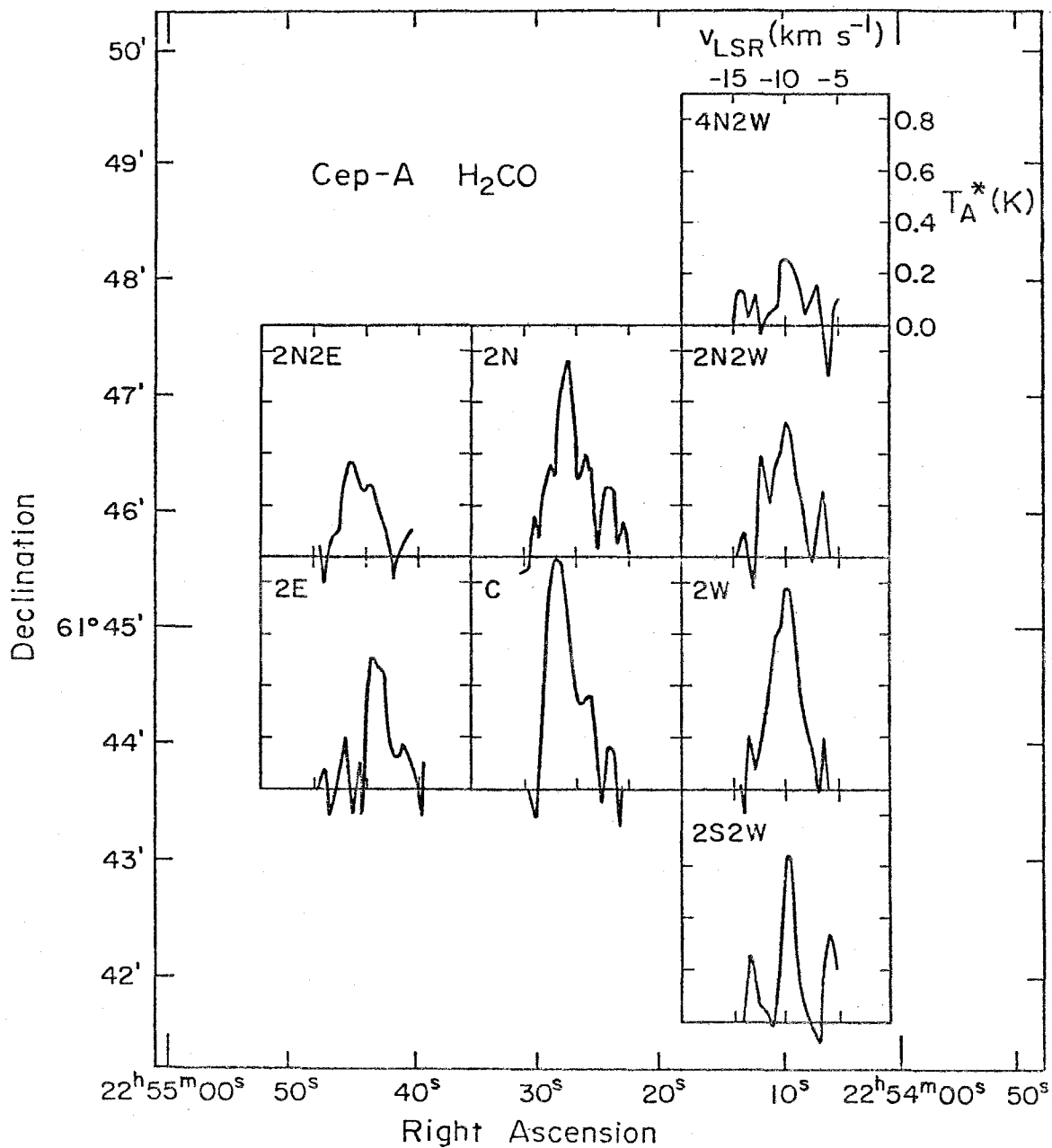


FIGURE 8a

Contours of $T_A^*(^{12}\text{CO})$ at $V_{\text{LSR}} = -12 \text{ km s}^{-1}$ for Cep-B.

The cross indicates the position of maximum $T_A^*(^{12}\text{CO})$.

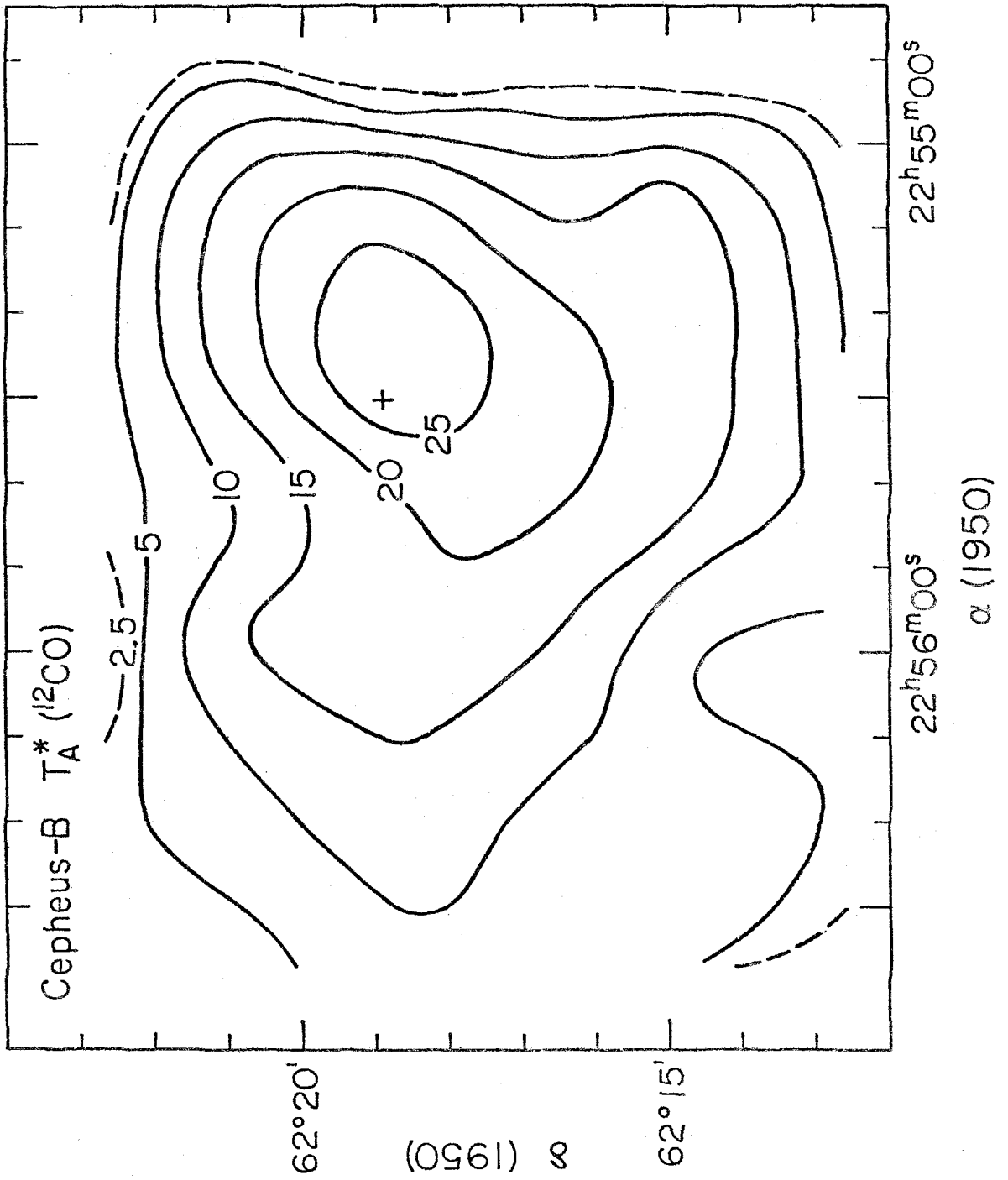
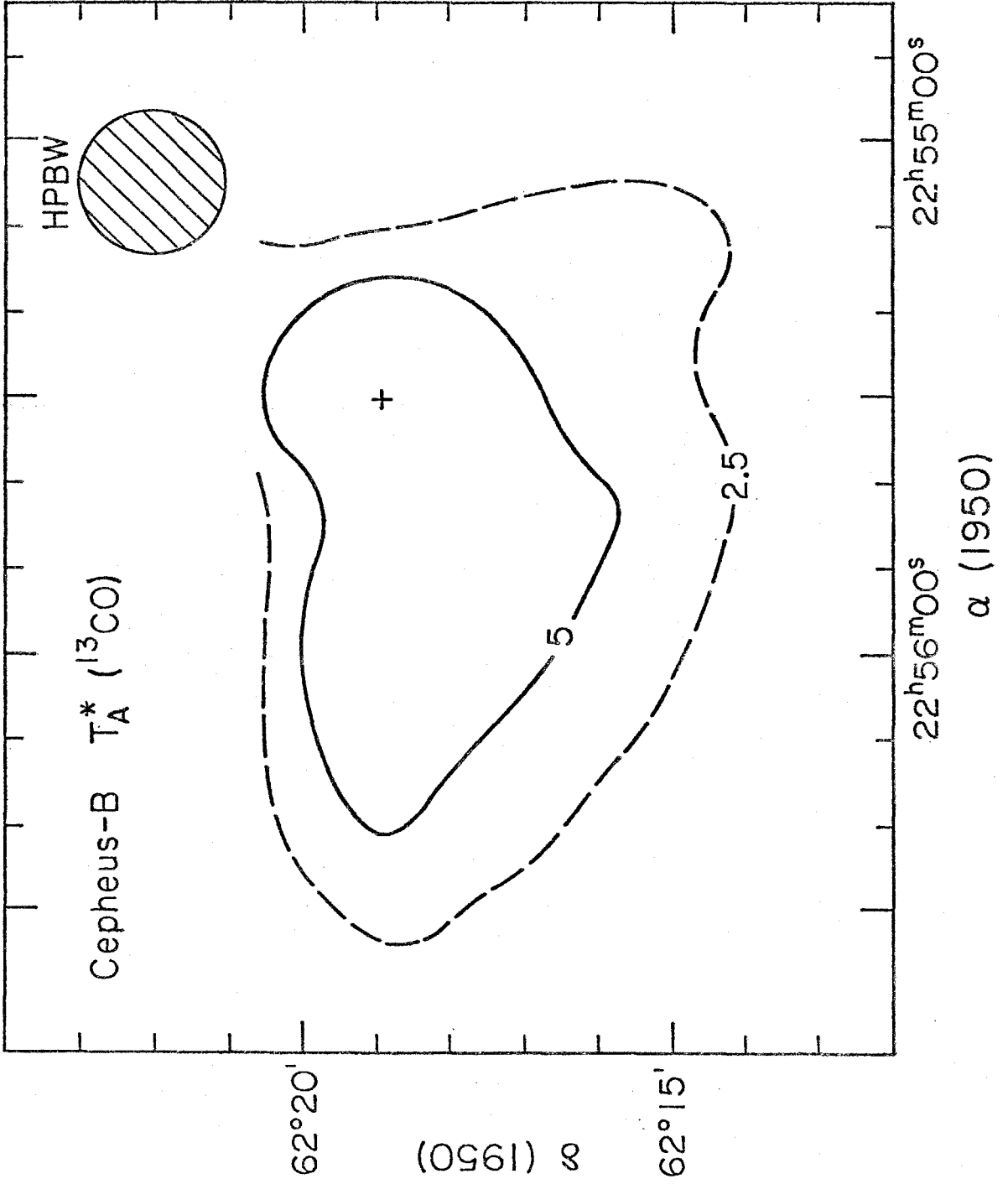


FIGURE 8b

Contours of $T_A^*(^{13}\text{CO})$ at $V_{\text{LSR}} = -12 \text{ km s}^{-1}$ for Cep-B.

A cross indicates the position of maximum $T_A^*(^{13}\text{CO})$.



-12.0 km s^{-1} , although at the boundary of the cloud itself (cf. Fig. 2), a feature at $\sim -15 \text{ km s}^{-1}$ remarked upon in § V is evident. Over the whole region the ratio $T_A^*(^{12}\text{CO})/T_A^*(^{13}\text{CO})$ is 3 - 5, and the ^{12}CO lines have widths at half-maximum of between 2 and 4 km s^{-1} . Limited searches of the region have been made in the 2-mm line of H_2CO but no detections have resulted.

c) Cepheus-C

Several velocity components are visible in the ^{12}CO profiles observed across Cep-C (cf. Figs. 4a, b, c, d). Over most of the region only one of these components, that at -10.3 km s^{-1} , is also seen in ^{13}CO . Contours of $T_A^*(^{12}\text{CO})$ and $T_A^*(^{13}\text{CO})$ are presented in Figures 9a and 9b. Maximum values of these quantities occur at different, although adjacent, positions as can be seen from the figures. The core of Cep-C probably encompasses both maxima since unambiguous detections of 2-mm H_2CO were made at their positions. From Table 2 it is clear that, in view of the observed $T_A^*(^{12}\text{CO})$, the values of $T_A^*(^{13}\text{CO})$ are unexpectedly high.

To the north and west of the central position shown in Figure 9a, a feature at -11.7 km s^{-1} gradually increases in strength. This northwest zone is in fact not unlike Cep-B in its general properties. Few ^{13}CO observations were made here since it is relatively far from the site of peak intensity, $\alpha = 23^{\text{h}}03^{\text{m}}38^{\text{s}}$, $\delta = +62^\circ 12' 23''$, but existing

FIGURE 9a

Contours of $T_A^*(^{12}\text{CO})$ at $V_{\text{LSR}} = -10.3 \text{ km s}^{-1}$ for Cep-C.

The cross indicates the position of maximum $T_A^*(^{12}\text{CO})$.

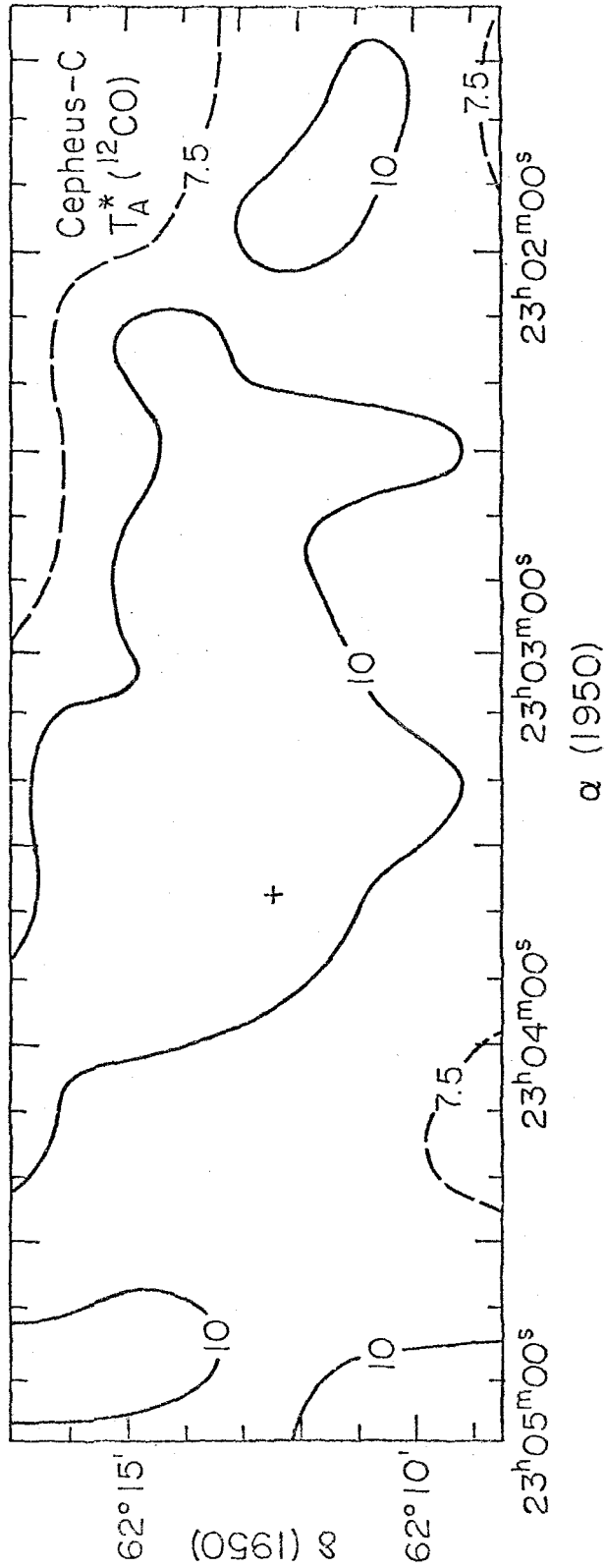
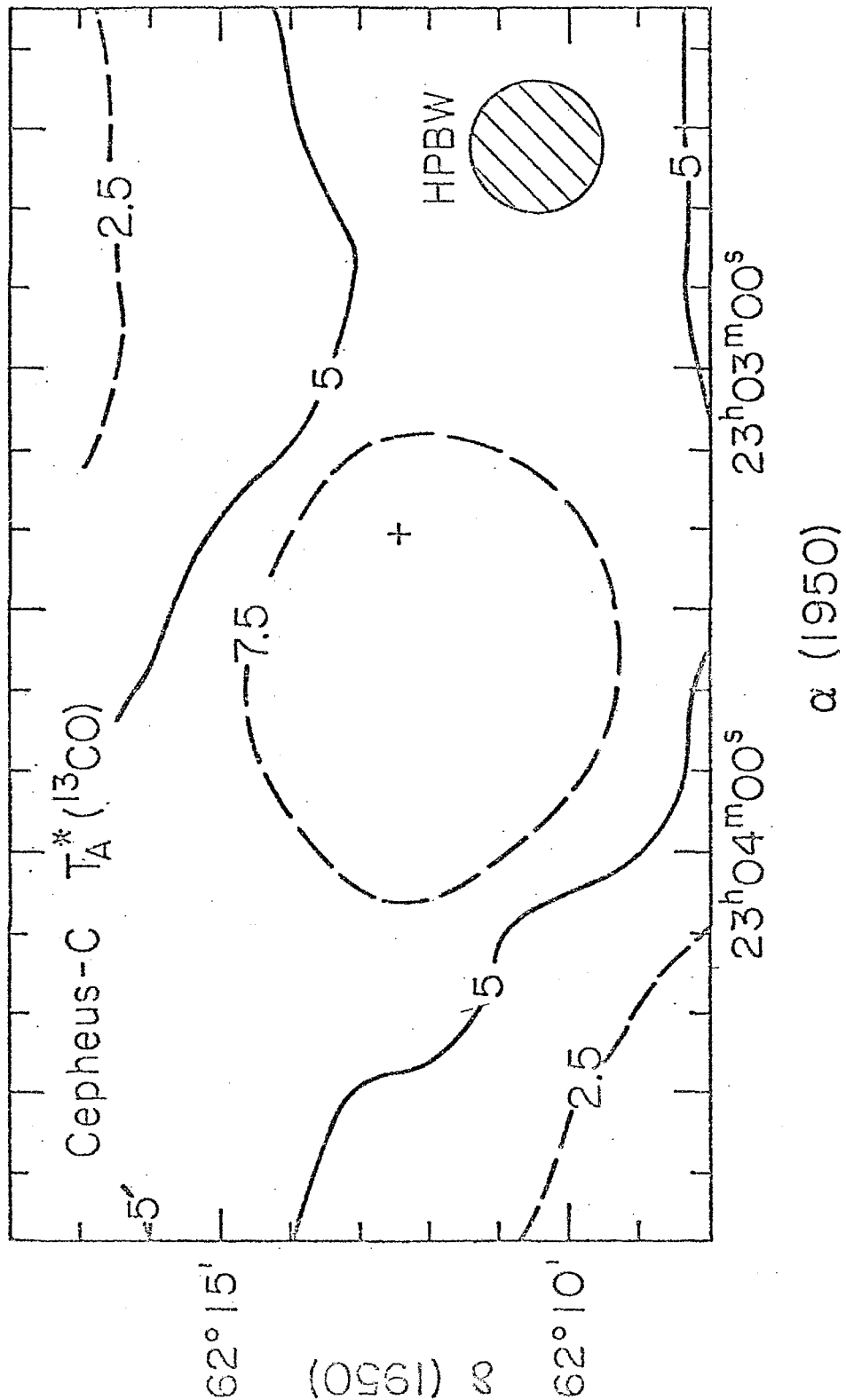


FIGURE 9b

Analogous contours of ^{13}CO . A cross indicates the position of maximum $T_A^*(^{13}\text{CO})$.



measurements indicate that the rarer isotope is never more than weakly present.

VII. SUMMARY

Detailed discussion and interpretation of the observations presented in this paper will be undertaken in Chapter 2. At this juncture the data will merely be summarized and indications will be given of the direction the analysis will take.

It has been demonstrated that in the vicinity of the young OB association Cepheus OB3 there is a large (20 pc \times 60 pc) molecular cloud complex comprising a number of components, several of which overlap in the line of sight. Emission from these components is seen at a number of velocities between -5 km s^{-1} and -15 km s^{-1} . Such velocities lie well within the range spanned by the association stars and the H II region S155, confirming the relationship between the cloud complex and the OB association.

Within this molecular cloud, from which Cepheus OB3 appears to have formed, three regions, Cep-A, -B and C, have particularly interesting properties. The interpretation of self-absorption profiles such as those seen in the direction of Cep-A is currently under discussion (Snell and Loren 1977; Leung and Brown 1977). It appears, however, that such profiles are observed at locations where new stars are currently forming. Intensity ratios and line widths over Cep-B are

typical of dark clouds heated by a single star (Milman 1975a, b; Dickman 1975). Simonson and van Someren Greve (1976) did in fact detect in the direction of Cep-B a small H I concentration which they concluded lay in front of S155 and was related to the dark clouds around Cepheus OB3. Observations in this direction made with the Westerbork Synthesis Radio Telescope at a wavelength of 6-cm indicate the presence of a weak extended (~ 30 arcseconds) H II region suggestive of an early B star (Israel 1977), but no other evidence for the existence of such a source in the form, for example, of an infrared object has been discovered. Searches (to 10 f.u. sensitivity) within each region for H₂O masers at the positions of peak ¹²CO intensity have yielded no detections (Knapp 1977).

Thus in the Cepheus cloud complex there is some evidence for the existence of an embedded star (Cep-B), a region of continuing star formation (Cep-A) and a zone Cep-C, which is perhaps the precursor of regions such as Cep-A and Cep-B.

It is clear that there is indeed a large amount of gas still associated with the stars of Cepheus OB3. Estimates of its mass relative to the member stars and neutral hydrogen in the association are of primary importance in considering the evolution of the complex. In view of the quantities of data involved and the very careful analysis necessary to determine the precise relationship between the

association and the molecular cloud the interpretation of the observations will be deferred until Chapter II.

REFERENCES

- Becklin, E. E., Neugebauer, G., and Wynn-Williams, C. G.
1973, Ap. J. (Letters), 182, L7.
- Beckwith, S., Evans, N. J. II, Becklin, E. E., and
Neugebauer, G. 1976, Ap. J., 202, 390.
- Blaauw, A. 1964, Ann. Rev. Astr. and Ap., 2, 213.
- Blaauw, A., Hiltner, W. A., and Johnson, H. L. 1959, Ap. J.,
130, 69.
- Crawford, D. L., and Barnes, J. V. 1970, A. J., 75, 952.
- Dickman, R. L. 1975, Ap. J., 202, 50.
- Downes, D., Winneberg, A., Goss, W. M., and Johansson,
L. E. B. 1975, Astr. Ap., 44, 243.
- Elmegreen, B. C., and Lada, C. J. 1977, A. J., 81, 1089.
- Garmany, C. 1973, A. J., 78, 185.
- Garrison, R. F. 1970, A. J., 75, 1001.
- Georgelin, Y. M. 1975, Thesis Universitie de Provence,
Observatoire de Marseilles.
- Harris, S. 1976, Ph.D. Dissertation, University of
Cambridge.
- Harris, S., and Wynn-Williams, C. G. 1976, M.N.R.A.S., 174,
649.
- Israel, F. P. 1977, private communication.
- Kester, D. 1977, private communication.
- Knapp, G. R. 1977, private communication.

- Kutner, M. L., and Tucker, K. D. 1975, Ap. J., 199, 79.
- Lada, C. J. 1976, Ap. J. Suppl., 32, 603.
- Leung, C. M., and Brown, R. L. 1977, Ap. J. (Letters), 214,
L73.
- Liszt, H. S., Wilson, R. W., Penzias, A. A., Jefferts,
K. B., and Wannier, P. G. 1974, Ap. J., 190, 557.
- Lucas, R., Encrenaz, P. J., and Falgarone, E. G. 1976,
Astr. Ap., 51, 469.
- Mezger, P. G., and Wink, J. E. 1975, H II Regions and
Related Topics, ed. T. L. Wilson and D. Downes
(New York: Springer-Verlag), p. 408.
- Miller, J. S. 1968, Ap. J., 151, 473.
- Milman, A. S., Knapp, G. R., Kerr, F. J., Knapp, S. L., and
Wilson, W. J. 1975a, A. J., 80, 93.
- Milman, A. S., Wilson, W. J., Knapp, G. R., and Knapp, S. L.
1975b, A. J., 80, 101.
- Simonson, S. G., and van Someren Greve, H. W. 1976, Astr.
Ap., 49, 343.
- Snell, R. L., and Loren, R. B. 1977, Ap. J., 211, 122.
- Ulich, B. L., and Haas, R. 1976, Ap. J. Suppl., 30, 247.
- Zuckerman, B., and Palmer, P. 1974, Ann. Rev. Astr. and Ap.,
12, 279.

CHAPTER 2

STAR FORMATION IN CEPHEUS OB3

I. INTRODUCTION

A molecular cloud complex related to the young OB association Cepheus OB3 has been detected. The observational data have been described in Chapter 1. Physical and kinematical properties of this cloud complex will now be derived, and discussed in conjunction with the observed properties of the association stars.

The Cepheus OB3 association is known to comprise two subgroups of stars (Blaauw 1964). Ages of these subgroups are recalculated; they are found to be of order $1-3 \times 10^5$ years and $5-7 \times 10^5$ years, a factor of ten lower than the values given by Blaauw (1964). Both subgroups appear to have formed at one end of the related molecular cloud.

The molecular cloud is estimated to have a mass of a few thousand solar masses, and its dimensions are 20 pc x 60 pc. It contains three smaller regions in which different stages of star formation may be identified. In one region there is evidence of the existence of an embedded star; another region appears to be currently collapsing to form a new subgroup of the association, while the third may be in a still earlier phase of collapse. The time scale for the formation of the new subgroup is comparable to the difference in age between the existing subgroups. All three regions lie at the same end of the molecular cloud as the birth-sites of the optically visible subgroups, and star

formation is apparently taking place at only one edge of the cloud.

The properties of the molecular cloud and of the regions of interest mentioned above are considered in § II. In § III the membership of the OB association and of its subgroups are critically examined, and the ages and sites of origin of these subgroups determined. Current interaction between the association stars and the molecular cloud is analyzed in § IV. In § V are considered ways in which star formation may have been initiated in this region, and how it propagates through the cloud. A summary and discussion of the results of the preceding sections are presented in § VI.

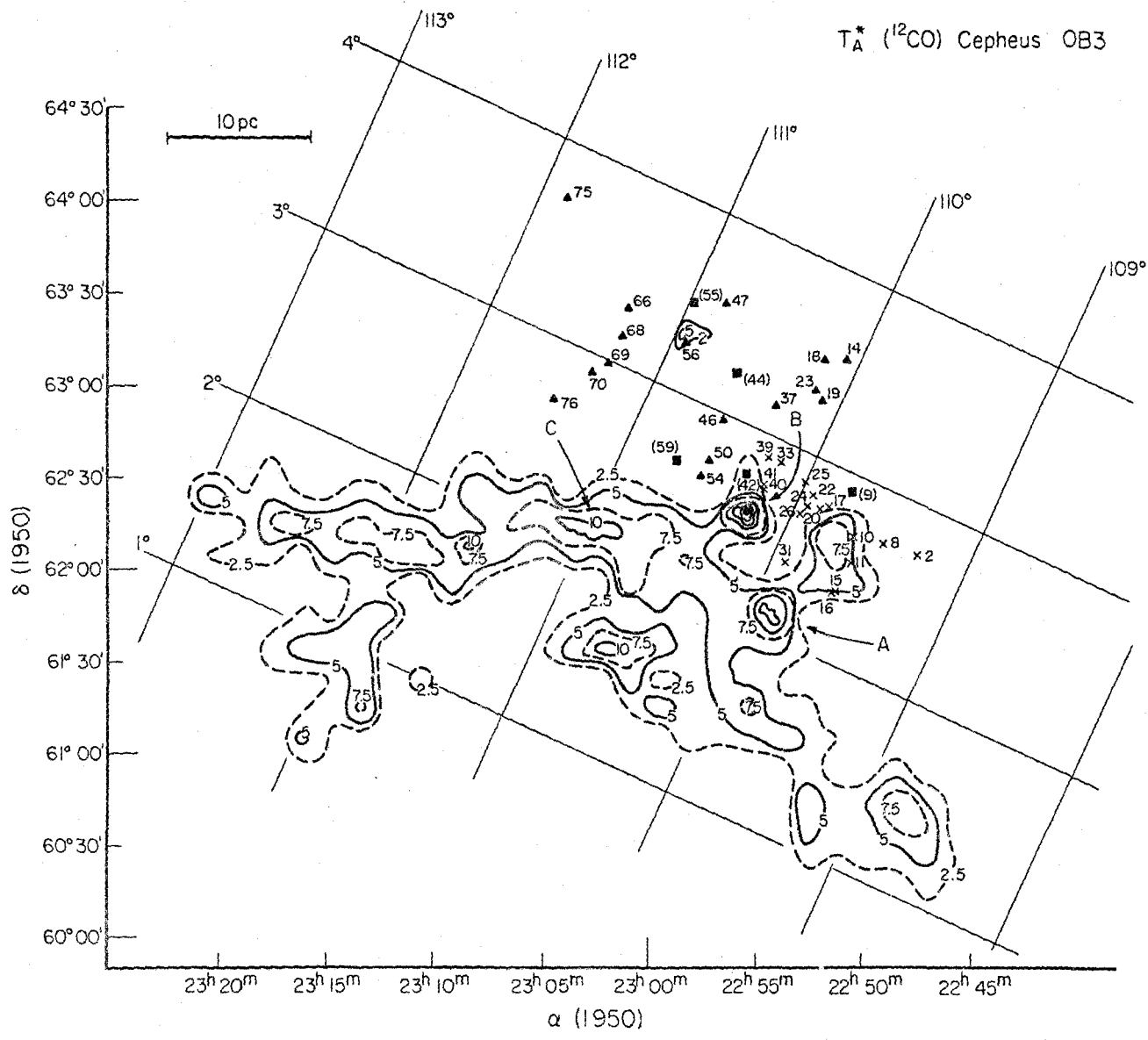
II. THE MOLECULAR CLOUD

In regions where stars have recently formed or are in the process of formation a variety of phenomena are noted in the associated molecular line observations. These include above average CO temperatures, CO profiles which are broadened or which display wide wings, density enhancement (indicated by the presence of such higher dipole moment molecules as H_2CO , HCN , CS) and, occasionally, self-absorption in the ^{12}CO profiles. Such phenomena have been noted in several regions of the Cepheus OB3 cloud complex. Contours of corrected antenna temperature, $T_A^*(^{12}\text{CO})$, resulting from the data of Chapter 1, are displayed in Figure 1. As

FIGURE 1

Contours of peak antenna temperatures, $T_A^*(^{12}\text{CO})$, for the Cepheus molecular cloud. The association stars are represented by crosses, filled triangles and filled squares. Crosses denote members of the younger subgroup, and filled triangles members of the older subgroup of Cepheus OB3. Filled squares represent stars unassigned to either subgroup. The numbering system is that of Blaauw, Hiltner and Johnson (1959).

T_A^* (^{12}CO) Cepheus OB3



in Figure 2 of Chapter 1, stars of the older and younger subgroups of the association are represented by filled triangles and crosses respectively. Filled squares denote possible additional members of the association. Following the terminology of Chapter 1, regions of particular interest are labeled -A, -B, and -C.

Observational evidence was presented in Chapter 1 indicating that in this cloud there exist an embedded star (Cep-B), a region of continuing star formation (Cep-A), and a zone (Cep-C) which may be the precursor of regions such as Cep-A. In regions where stars are being created it is important to ascertain how much mass is available for star formation and if the individual regions are gravitationally unstable. The properties of these areas, and of the cloud as a whole, will now be considered.

a) Densities

In Table 1 observed and derived parameters for Cep-A, -B and -C are presented together with results for the entire molecular cloud. Observed properties at the positions of peak intensity in each region are reproduced from Chapter 1. The derivation of ^{13}CO column densities, $N(^{13}\text{CO})$, and molecular hydrogen column densities $N(\text{H}_2)$, will be described below. Corresponding volume densities $n(^{12}\text{CO})$ and $n(\text{H}_2)$, will also be discussed. Mean values, $\langle N(^{13}\text{CO}) \rangle$, were obtained by averaging all available measures within the 10 K

TABLE 1
REGIONAL AND CLOUD PARAMETERS

			Cep-A	Cep-B	Cep-C	Cloud
^{12}CO	T_A^*	K	18.0:	29.0	13.4	
	V	km s^{-1}	-12:	-12.3	-10.3	
^{13}CO	T_A^*	K	11.5	8.1	9.1 ^a	
	V	km s^{-1}	-10.3	-12.3	-10.3 ^a	
	ΔV	km s^{-1}	3.2	1.9	2.4 ^a	
Area	15K	pc^2	1.04	1.86	... ^b	261 ^c
	10K	pc^2	4.78	3.03	3.23	
$N(^{13}\text{CO})$		cm^{-2}	$5-7 \times 10^{16}$	$2-3 \times 10^{16}$	$3-4 \times 10^{16}$	
$N(\text{H}_2)_{\text{peak}}$		cm^{-2}	$2-4 \times 10^{22}$	$1-2 \times 10^{22}$	$1-2 \times 10^{22}$	
$n(\text{H}_2)_{\text{peak}}$		cm^{-3}	$7-11 \times 10^3$	$3-4 \times 10^3$... ^b	
$\langle N(^{13}\text{CO}) \rangle$		cm^{-2}	$2-3 \times 10^{16}$	1×10^{16}	$2-3 \times 10^{16}$	5×10^{15}
$\langle N(\text{H}_2) \rangle$		cm^{-2}	1×10^{22}	6×10^{21}	1×10^{22}	
$\langle n(\text{H}_2) \rangle$		cm^{-3}	$2-4 \times 10^3$	1×10^3	$2-4 \times 10^3$	
Mass		M_{\odot}	500	100	300	5×10^3

Footnotes to Table 1:

- a - ^{13}CO values at position of ^{12}CO peak
- b - No 15K contours exist.
- c - Total area inside 5K contours

contours. The areas covered by relevant contours are also given, assuming the distance to the association is 725 pc (Crawford and Barnes 1970).

There are a large number of uncertainties involved in the determination of the densities. Molecular hydrogen, the most abundant constituent of molecular clouds, is unobservable at millimeter wavelengths. Its column density must therefore be derived from the column density of observable molecules, usually ^{12}CO and ^{13}CO . The first uncertainties in the calculations are introduced in determining $N(^{13}\text{CO})$, since it is usual to assume that ^{13}CO is thermalized and that the excitation temperatures of the $J = 1 \rightarrow 0$ transition are the same for ^{12}CO and ^{13}CO .

For a region with uniform T_{01} along the line of sight, where T_{01} is the excitation temperature of the $J = 1 \rightarrow 0$ transition of CO,

$$T_A^*(^{12}\text{CO}) = \frac{h\nu}{k} [F(T_{01}) - F(T_{bb})] (1 - e^{-\tau}) \quad (1)$$

Here $T_A^*(^{12}\text{CO})$ is the corrected antenna temperature, $F(T) = (e^{h\nu/kT} - 1)^{-1}$, T_{bb} is the 2.7 K background radiation and τ is the optical depth. At H_2 densities of 10^3 cm^{-3} or higher, typical of molecular clouds, ^{12}CO is thermalized and optically thick (Penzias et al. 1971) and $\tau(^{12}\text{CO}) \gg 1$. A similar relation to equation (1) holds for ^{13}CO , with the difference that the rarer isotope is optically thin, so that

$\tau(^{13}\text{CO})$ may be determined if $T_{01}(^{12}\text{CO}) = T_{01}(^{13}\text{CO})$.

The column density of ^{13}CO molecules in the $J = 0$ state, N_0 , is related to the optical depth by

$$\tau_\nu = \frac{3}{8\pi} \frac{c^2}{\nu^2 \Delta\nu} AN_0 (1 - e^{-h\nu/kT_{01}}), \quad (2)$$

where ν is the frequency of the observed line, and $\Delta\nu$ is its frequency width at half-maximum; $A = \frac{64\pi^4 \nu^3 \mu^2}{9hc^3}$, and for CO the dipole moment $\mu = 0.112$ debyes (Lovas and Tiemann 1974).

Assuming a Boltzmann distribution the number of molecules in all states, $N(^{13}\text{CO})$, can be obtained from the number in the ground state through $N(^{13}\text{CO}) = \frac{N_0 T_{01}}{2.767}$. The derivation of this relation requires that the sum over J be replaced by an integral in the formula for the linear molecule partition function, $Q = \sum_{J=0}^{\infty} (2J+1) e^{-E_J/kT_{\text{kin}}}$. Assuming LTE holds, the kinetic energy of the cloud, T_{kin} , is equal to T_{01} .

E_J , the energy of the J^{th} rotational level is equal to $J(J+1)hB$, where B is the rotation constant of the molecule.

Numerical comparisons between sums and integrals over J for a number of cases demonstrate that the replacement of T_{01} by $(T_{01} + 0.9)$ in this formula for $N(^{13}\text{CO})$ compensates for the approximation of the sum by an integral. Substituting for N_0 in equation (2), and expressing the half-width in terms of velocity rather than frequency leads to the following expression for the column density of ^{13}CO ,

$$N(^{13}\text{CO}) = \frac{2.312 \times 10^{14} \tau(^{13}\text{CO}) \Delta V(^{13}\text{CO}) (T_{01} + 0.9)}{(1 - e^{-5.291/T_{01}})} \text{ cm}^{-2}, (3)$$

where $\Delta V(^{13}\text{CO})$ is the velocity width at half-maximum of the ^{13}CO line.

An alternative method of obtaining $N(^{13}\text{CO})$ has been devised by Blair (1976) to circumvent the difficulty of equating $T_{01}(^{13}\text{CO})$ with $T_{01}(^{12}\text{CO})$. He relates $N(^{13}\text{CO})$ to $\tau(^{13}\text{CO})$ through the mass absorption coefficient and finds

$$N(^{13}\text{CO}) = 3.6 \times 10^{14} \Delta V(^{13}\text{CO}) T_A^*(^{13}\text{CO})/f_1, \quad (4)$$

where f_1 is the fraction of ^{13}CO molecules in the $J = 1$ state. Solving the equations of statistical equilibrium and radiative transfer in a large velocity gradient model (see Snell and Loren 1977), Blair shows that f_1 takes values between 0.26 and 0.55, approaching the former value at densities greater than 10^4 cm^{-3} .

Very similar values of $N(^{13}\text{CO})$ result from applying equations (3) and (4) to the observed data, although equation (3) consistently leads to slightly smaller column densities. Any noticeable ranges in value are indicated in Table 1. Blair's method still requires the assumption that ^{13}CO is thermalized and observations indicate that this is not the case at densities $\lesssim 10^3 \text{ cm}^{-3}$ (see for example, Dickman 1976). However, from his model calculations he concludes that, even in very diffuse regions, use of

$f_1 = 0.26$ will result in column densities which are in error by a factor of 2 at most. The column densities of Table 1 will be taken to be correct to within this factor.

Computation of $N(\text{H}_2)$ from $N(^{13}\text{CO})$ necessitates the introduction of further assumptions. Here Dickman's (1976) relation

$$N(\text{H}_2) = (5.0 \pm 2.5) \times 10^5 N(^{13}\text{CO}) \quad , \quad (5)$$

will be applied.

Equation (5) is based on Dickman's finding that within the range $1.0^m < A_v < 4.0^m$, and probably up to $A_v = 10.0^m$, a linear relation,

$$A_v/N(^{13}\text{CO}) = 4.0 \times 10^{-16} \text{ cm}^2 \text{ mag} \quad , \quad (6)$$

exists between the visual extinction, A_v , determined from star counts and $N(^{13}\text{CO})$, determined as in equation (3) above. It is known that $N_{\text{total}}/A_v = 2.50 \times 10^{21} \text{ cm}^{-2} \text{ mag}^{-1}$ (Jenkins and Savage 1974), where N_{total} is the total number of particles (HI, H_2 , protons) in the line of sight, in lower density molecular gas and H I clouds. Therefore

$$N(\text{H}_2)/A_v \approx 1.25 \times 10^{21} \text{ mols cm}^{-2} \text{ mag}^{-1} \quad , \quad (7)$$

and $N(\text{H}_2)$ may be directly related to $N(^{13}\text{CO})$ by equation (5). Values of $N(\text{H}_2)$ in Table 1 are thus derived employing only the plausible assumptions that the normal gas to dust

ratio pertains in the region observed and that there is complete conversion of atomic hydrogen to molecular hydrogen in the line of sight (cf. Hollenbach et al. 1971).

This way of determining $N(\text{H}_2)$ is more reliable than methods whose application require knowledge of such uncertain quantities as the $^{12}\text{CO}/^{13}\text{CO}$ isotope ratio, the fraction of carbon present in the form of CO and the C/H abundance ratio (cf. Elmegreen and Lada 1977a).

Average volume densities, $\langle n_{\text{H}_2} \rangle$, were obtained from the column densities assuming each source to have a line of sight depth equal to the square root of the surface area enclosed by the 15 K contour. These are shown in Table 1. For peak values of n_{H_2} the line of sight depth was taken to be equal to the square root of the surface area enclosed by the contour of highest temperature in the region.

Densities were also derived from formaldehyde observations. 2mm H_2CO results at the peak of Cep-A are given in Chapter 1. One measure of 2 cm H_2CO ($T_A^* = -0.11$ K) has been made at this position. A comparison of these results with the models of Evans and Kutner (1976) implies a peak density of $\sim 6 \times 10^4 \text{ cm}^{-3}$. The difference between this density and that derived from ^{12}CO and ^{13}CO observations, $\lesssim 10^4 \text{ cm}^{-3}$, is too large to be explained by errors in the line of sight depth. Evans et al. (1977) have noted a similar situation in S255. There the H_2CO data lead to

densities one hundred times higher than those determined from CO data.

Blair et al. (1977) and Wootten et al. (1977) have proposed that in the denser regions of molecular clouds ^{12}CO , ^{13}CO , H_2CO and HCO^+ are depleted relative to H_2 . Equation (5) would then be invalid in these regions. The former authors base their assertions on model fitting to observed lines in the S140 cloud, while the latter have studied the HCO^+ observations in a number of molecular clouds of different densities. They find $n(^{13}\text{CO})/n(\text{H}_2) = 2 \times 10^{-7}$, as compared with Dickman's (1976) value 2×10^{-6} . This degree of depletion of ^{13}CO in the core of Cep-A would explain the disagreement between densities from H_2CO and ^{13}CO data, since the latter determination was based on Dickman's relation. A value of $\sim 6 \times 10^4 \text{ cm}^{-3}$ is therefore accepted for the peak density in Cep-A. However, while equation (5) may be invalid in the very dense core of any region, it is probably applicable over most of Cep-A, -B and -C, and there is no reason to doubt the average densities given in Table 1.

b) Masses

Before masses can be calculated, the geometry of the sources involved must be specified. The usual technique has been to assume a spherically symmetric source whose diameter is equal to the square root of its visible surface area. For Cep-A, -B and -C the 10 K contours define the

surface areas. Evans et al. (1976) have adopted a slightly different approach, determining masses from the product of the average column density and the projected surface area of the source. Both forms of mass determination were applied to the data for Cep-A, -B and -C, with very similar results. These are displayed in Table 1.

The total mass of the cloud was calculated by assuming that over the area bounded by the 5 K contours (261 pc^2) the mean ^{13}CO column density = $5.1 \times 10^{15} \text{ cm}^{-2}$. This value derives from the average of all column densities observed across the cloud, individual regions being weighted according to the square of their surface areas. The mass is also shown in Table 1.

c) The Nature of Cep-A, Cep-B and Cep-C

The derived areas, densities and masses of Cep-A, Cep-B and Cep-C will now be used in conjunction with their observed intensities and line widths to justify the earlier suggestion that these regions are sites of star formation.

From Chapter 1 it will be recalled that the ^{12}CO profiles in the central region of Cep-A are self-absorbed, the velocity of the self-absorption minimum being displaced from that of the ^{13}CO maximum by 1.4 km s^{-1} . The variation of the phenomenon across Cep-A may be seen in Figure 5 of Chapter 1, but for illustration the ^{12}CO

profile and its ^{13}CO counterpart at the center of Cep-A are shown in Figure 2. Snell and Loren (1977) have suggested that such profiles are indicative of the collapse of a given region. If their hypothesis is accepted, the profiles observed across Cep-A fulfill the necessary criteria for a collapsing region. It should, however, be noted that Leung and Brown (1977) have pointed out that such profiles do not necessarily indicate collapse.

Most self-absorbed profiles detected to date have been seen in the direction of embedded stars (Loren, Peters and Vanden Bout 1974; Encrenaz, Falgarone and Lucas 1975; Kutner and Tucker 1975; Knapp et al. 1976; Loren 1976). In Cep-A there is little proof of the presence of an embedded star. A few minutes west of the region a feature resembling a reflection nebula is visible on the PSS plates. This becomes even more apparent on plates at 8200 \AA . While it may be due to an embedded protostar in Cep-A, limited searches in the near infrared have not produced corroborative evidence for such a source.

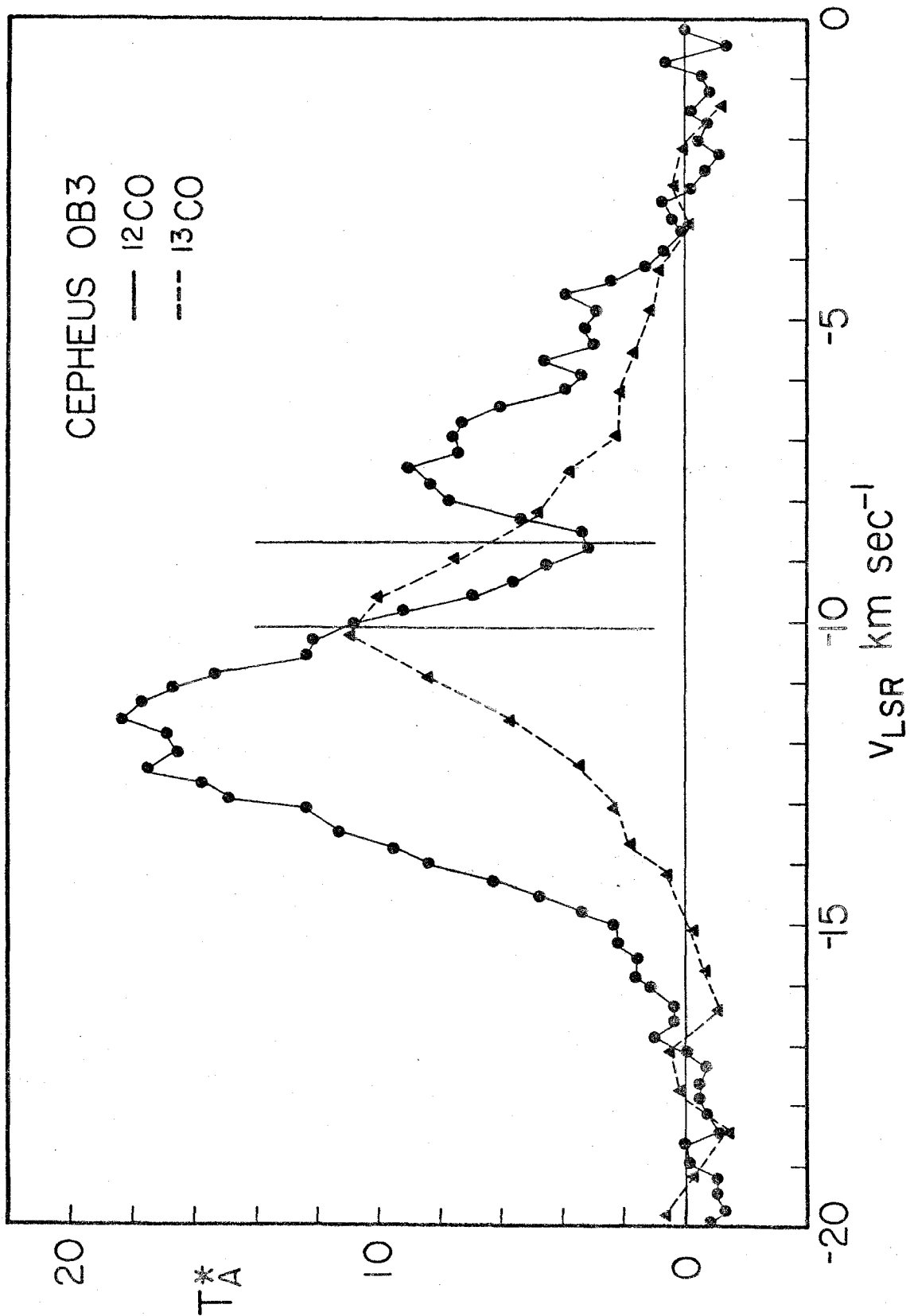
Some measure of the stability of a region is given by comparing its Jeans length, $\lambda_{J/2}$, with its radius.

$$\lambda_{J/2} \approx 0.81 \left(\frac{T_{\text{kin}} R^3}{M} \right)^{1/2} \text{ pc} \quad (\text{Dickman 1976}),$$

where T is the kinetic temperature of the region, R its radius in parsecs, and M its mass in units of solar mass.

FIGURE 2

^{12}CO and ^{13}CO profiles observed at the center of Cep-A. Vertical lines indicate the positions of the ^{12}CO minimum and the ^{13}CO maximum.



It seems likely that Cep-A is in a state of gravitational collapse, since its Jeans length is 0.5 pc, a factor of more than four less than its radius, and there is no evidence of an embedded source to cause internal expansion. The free-fall velocity at its boundary, given by $(\frac{2GM}{R})^{1/2}$, is 1.4 km s^{-1} , in excellent agreement with the velocity difference between the ^{13}CO peak and the ^{12}CO absorption dip. This difference is a measure of the maximum infall velocity at the edge of a cloud in which self-absorption is observed. The free-fall collapse time is of order $\frac{3 \times 10^7}{\sqrt{n_{\text{H}_2}}}$. Adopting $\langle n_{\text{H}_2} \rangle = 4.3 \times 10^3 \text{ cm}^{-3}$ leads to $\sim 5 \times 10^5$ years. However, a density of $n_{\text{H}_2} \sim 6 \times 10^4 \text{ cm}^{-3}$ is inferred from observations of 2 mm and 2 cm H_2CO in the central region, with a corresponding collapse time of $\sim 1 \times 10^5$ years. Since the larger density appears to exist over only a small central part of Cep-A, the time scale for collapse is probably somewhat less than 5×10^5 years.

The mass of Cep-A is of the order of $500 M_{\odot}$, considerably lower than the $2000 M_{\odot}$ quoted by Blaauw (1964) as typical for individual subgroups of an OB association. Blaauw's mass estimate was derived by extrapolating from the visible stars by means of the Initial Luminosity Function, assuming that there were also present less massive and as yet invisible members of the associations. It may well be that the luminosity function for OB associations

is quite different from the Initial Luminosity Function. Recent investigations (see Elmegreen and Lada 1977b and references therein) have in fact indicated that O and B stars may form under different conditions from lower mass stars. The total mass of an individual subgroup would then be close to the sum of the masses of the constituent stars. From Garrison's (1970) spectral classifications, estimates can be made of the stellar masses in Cepheus OB3 (Harris *et al.* 1963; Underhill 1966). The masses of the older and younger subgroups are found to be $\sim 200 M_{\odot}$ and $\sim 300 M_{\odot}$ respectively. Conti and Burnichon (1975) have shown that 20% of all O stars have masses greater than $60 M_{\odot}$, but a typical subgroup of 15 stars, comprising a few very high mass O stars and lower mass O and B stars could easily be formed from the $500 M_{\odot}$ available in Cep-A. It is postulated that Cep-A is collapsing on a time scale of a few $\times 10^5$ years to form a new subgroup of the Cepheus OB3 association.

In Cep-C no self-absorption is detected but the ^{12}CO lines are broader than those usually seen in dark clouds and ^{13}CO is markedly enhanced relative to its ^{12}CO value (see Table 2, Chapter 1). Around the center of the region weak ($\lesssim 0.6$ K) 2 mm H_2CO emission is present. Similar emission has been observed by Evans and Kutner (1976) in the Taurus and L134N dark clouds. Although there are no other indications of density enhancement, such as IR sources

or even CO hotspots, Evans and Kutner, using spatially coincident measurements of 2 cm and 6 cm H₂CO absorption, have shown that densities of $n_{\text{H}_2} \sim 10^4 \text{ cm}^{-3}$ must exist in these clouds at the locations where 2 mm H₂CO emission is present. Thus, although observations of 2 cm or 6 cm H₂CO are lacking, the presence of 2 mm H₂CO is evidence for densities of order 10^4 cm^{-3} in the center of Cep-C. As in the case of Cep-A, this is considerably larger than the peak density calculated from the ¹²CO and ¹³CO measurements (see Table 1) and the remarks in § IIa concerning differences between relative abundances of heavy molecules in dense molecular clouds and dark clouds are applicable.

The radius and mass of Cep-C are rather smaller than Cep-A (see Table 1), but its Jeans length is a factor of four smaller than its radius, so that it could be in a state of gravitational collapse. A free-fall collapse time slightly greater than that for Cep-A results, the velocity at the boundary being $\sim 1.2 \text{ km s}^{-1}$. The presence of the dense core, the likelihood that the region is collapsing, and the generally weaker and narrower profiles as compared with Cep-A, indicate that Cep-C may be the precursor of a region such as Cep-A.

The mass derived for Cep-B is only $\sim 100 M_{\odot}$. Clearly this is not the formation site of a new subgroup. There is no evidence for density enhancement either in the form of

broadened ^{12}CO profiles or detectable 2 mm H_2CO . The Jeans length of the region is comparable to its radius and gravitational collapse is improbable. Here, however, the ^{12}CO intensities attain their highest values in the Cepheus OB3 cloud. The lines remain relatively narrow and observations across the region are typical of those seen in a dark cloud heated by a single star. From Figure 1 it can be seen that Cep-B is a reasonable position for a still embedded association star. The average extinction in the region can be determined using $A_V = (4.0 \pm 2.0) \times 10^{-16} N(^{13}\text{CO})$ (Dickman 1976), and is found to be of order 5 magnitudes. Further evidence for the existence of such a star will be given in § IIId.

d) Heating and Cooling Rates for the Molecular Cloud

Energetics of the gas and dust in the Cepheus cloud will now be investigated. Goldreich and Kwan (1974) attribute the heating of molecular gas at densities greater than $n_{\text{H}_2} = 10^4 \text{ cm}^{-3}$ to collisions between H_2 molecules and dust grains. Scoville and Kwan (1976), however, cite observational evidence to demonstrate that the kinematic temperature of the gas, T_{kin} , is often quite close to the dust temperature, T_d , and point out that this process can, at densities $n_{\text{H}_2} \sim 10^4 \text{ cm}^{-3}$ produce only $T_{\text{kin}} \approx 1/2 T_d$. They show that the heating rate will be increased if H_2O molecules absorb far infrared radiation from the dust and

subsequently de-excite through collisions with H_2 . The resulting gas and dust will then be thermally coupled at $n_{H_2} \sim 10^4 \text{ cm}^{-2}$. In both theories it is presumed that the gas is heated by the dust. Since no far infrared measurements of this cloud have yet been made, T_d is unknown and other sources of gas heating may be relevant here.

Total cooling rates for the gas and dust are determined for Cep-A, Cep-B and Cep-C by summing, as did Evans et al. (1977) for S255, contributions from concentric shells around each source bounded by contours 10 K, 15 K, etc. For the 10 K and 15 K shells the projected areas on the plane of the sky are given in Table 1. Values of T_{kin} appropriate to each contour value of $T_A^*(^{12}\text{CO})$ are shown in Table 2.

Cooling of the molecular gas is affected principally through CO emission, and for densities $n_{CO} n_{H_2} \gg 10^2 \text{ cm}^{-6}$ the cooling rate is $\Lambda(\text{CO}) = 2 \times 10^{-27} T_{kin}^3 \text{ ergs cm}^{-3} \text{ s}^{-1}$ (Scoville et al. 1975). For each source, total gas cooling rates, $\sum_i \Lambda_i \Delta v_i$, where Δv_i is the volume of each contributing shell, are given in column 2 of Table 3.

In the absence of far infrared observations estimates of the dust cooling rates must be inferred from the ^{13}CO data. Evans et al. (1977) derived an empirical relation, $\tau_{FIR} \approx 10^{-18} N(^{13}\text{CO})$, between the far infrared optical depth, τ_{FIR} , and the ^{13}CO column density $N(^{13}\text{CO})$. It appears to agree fairly well with available observational

TABLE 2
KINETIC TEMPERATURE

T_A^* (^{12}CO) (k)	T_{kin} (K)
25	28.5
20	23.5
15	18.4
10	13.4
5	8.3

TABLE 3

HEATING AND COOLING RATES IN THE CLOUD

(1)	$\sum_i \Lambda_i \Delta v_i$ (L_{\odot})	τ_{FIR} (pk) (3)	τ_{FIR} (mean) (4)	$\sum_i C_i$ (FIR) (L_{\odot}) (5)
Cep-A	0.5	0.049	0.02	4.6×10^3
Cep-B	0.3	0.021	0.01	4.2×10^3
Cep-C	0.1	0.030	0.02	1×10^3

data and will be employed here. In Table 3 the values of τ_{FIR} at the peak of each source, and averaged over the source are displayed in columns (3) and (4) respectively. Dust cooling rates are in column (5). Clearly considerably more energy is radiated by the dust than by the gas.

As already noted, T_d is unknown here, but since dust cooling of the gas is very efficient (Scalo 1977), it must be at least equal to T_{kin} . Some source of dust heating is therefore required. Embedded near infrared objects can provide the necessary energy, but no such sources are known in the Cepheus OB3 cloud.

It was proposed in § IIc that an embedded early B star might exist in Cep-B. If this region is heated by one star the luminosity of each shell should be the same. For the 25 K, 20 K, 15 K and 10 K shells of Cep-B the respective luminosities are $1.5 \times 10^3 L_{\odot}$, $1.1 \times 10^3 L_{\odot}$, $1.1 \times 10^3 L_{\odot}$ and $0.5 \times 10^3 L_{\odot}$. The first value may be too high since it was derived assuming that $\tau_{\text{FIR}}(\text{pk})$ applied throughout the 25 K shell, whereas $N(^{13}\text{CO})$, and therefore τ_{FIR} , falls off rather quickly in this region. Irregularities within the 10 K shell could equally account for the rather low luminosity found there, and it is concluded that an embedded star may be present. A star of spectral type B2 with luminosity $\sim 5 \times 10^3 M_{\odot}$ (Panagia 1973) would provide just sufficient energy to balance the dust cooling rate.

However, if such a star exists in Cep-B the extinction in this direction must be considerably larger than the 5 magnitudes derived in § IIc.

Sources of heat for the dust over most of the cloud are not obvious, although the proximity of the younger subgroup stars to the cloud suggests that they may contribute largely to its heating. No detailed calculations concerning the effects of stellar radiation on the dust temperature have been made, since the mechanism of heat transfer from external sources to the cloud is not well understood and since T_d is in any case a weak function of distance from the star (Scoville et al. 1975). However, the stellar contribution to dust heating may be roughly estimated by considering the effect of the radiation from the younger subgroup on unshielded grains at the cloud edge. The spectral types (Garrison 1970) of its members imply a total luminosity (Panagia 1973) $\sim 5 \times 10^5 L_\odot$ for the younger subgroup. Taking the mean distance between these stars and the cloud edge to be 3 pc, this luminosity could produce a grain temperature of 13 K. Throughout most of the cloud the gas kinetic temperature is in fact lower than 13 K. It is therefore possible that the gas is heated by dust, and the association stars contribute significantly to the heating of the dust itself.

III. THE CEPHEUS OB3 STARS

In principle if a star's age and its proper motion are known, it is possible to ascertain how far it has moved on the plane of the sky since its formation. In practice the errors inherent in the proper motions are very large, and often only an upper limit to the age is known, so that such a calculation is not particularly significant for individual stars. In OB associations, however, the stars are thought to be expanding away from a common origin, and an "expansion age", corresponding to the time which has elapsed since they began to move away from each other, may be computed. Proper motion errors still preclude a precise determination of the birthplace, but the general area in which it is situated may be identified. Before the origins of the Cepheus OB3 association can be established, membership in the association and in its individual subgroups, as well as the ages of these subgroups, must be critically examined.

a) Association Membership

A list of members of the Cepheus OB3 association was originally given by Blaauw et al. (1959). Membership was decided on the basis of location on the color-magnitude diagram, distribution on the sky and interstellar extinction. Blaauw et al. found that stars with $(B-V)_0$ less than $0.^m15$ have an average interstellar extinction $\bar{A}_V = 2.^m46$, and are more concentrated on the plane of the sky than those

with $(B-V)_0$ greater than $0.^m15$, which have an average extinction $\bar{A}_V = 1.^m25$. They concluded that stars having $(B-V)_0 < 0.^m15$ belonged to the association but membership of other stars was not entirely excluded. The positions of the association stars are shown in Figure 1.

Two stars in the original list, BHJ 44 and BHJ 59, were not included as members in a later study of proper motions and radial velocities in the association (Garmany 1973). Since they fit the above membership criteria in all respects, these stars will be considered to be members for the purposes of this analysis. Because it is difficult to assign them to either subgroup (see § IIIb), their positions are shown as filled squares in Figure 1.

In the solar neighborhood the density of early type stars is $0.48 \times 10^{-8} \text{ pc}^{-3}$ for O5 stars, increasing to $164 \times 10^{-8} \text{ pc}^{-3}$ for B5 stars (Prentice and Ter Haar 1969; Torres-Peimbert et al. 1974; Cruz-Gonzalez et al. 1974). Within the Cepheus OB3 boundaries the number of O stars expected is 3×10^{-5} and B5 stars is 1.1×10^{-2} . Stars in the Cepheus region of spectral type B5 or earlier, having the appropriate distance modulus, $9.^m3$, (Crawford and Barnes 1970), are therefore very likely to be association members. However, the uncertain distance modulus of BHJ 11 coupled with its location on the HR diagram and its unusually high extinction, $4.^m3$, render its membership very doubtful.

b) Subgroup Membership

The members of each subgroup of Cepheus OB3 listed by Garmany (1973) are given in Table 4. If there is any doubt that an individual star belongs to the association or to the particular subgroup (see discussion following) its BHJ number is enclosed in parentheses. BHJ 44 and BHJ 59 are classified as older subgroup members (see below).

Association stars are assigned to separate subgroups on the basis of their position in the Hertzsprung-Russell diagram and their relative concentration on the plane of the sky (Blaauw 1958). In general the earliest spectral types are found in the more densely populated areas of the associations. The more dispersed stars are of later spectral type or at systematically higher luminosities than those of the same spectral types lying in the denser regions. The subgroups should therefore represent groups of stars of different ages. Since the boundary of the "densely populated" region of the association is not precise, it is obvious that there will be stars which can almost equally well be assigned to either subgroup.

In an attempt to distinguish more clearly between stars of each subgroup, the distribution of spectral types, interstellar extinctions, radial velocities and proper motions among the stars are displayed in Figures 3a through 3e respectively. Hatched areas represent the older subgroup

TABLE 4
SUBGROUPS OF CEPHEUS OB3

Younger Subgroup				Older Subgroup			
2	16	(25)	40	14	(44)	56	70
8	17	26	41	18	46	(59)	75
10	20	31		19	47	(66)	76
(11)	22	(33)		23	(50)	68	
15	24	(39)		(37)	54	69	

FIGURE 3a .

Distribution of spectral types among the Cepheus OB3 stars. Hatched regions indicate older subgroup stars. Cross-hatched regions represent older subgroup stars of luminosity class other than V.

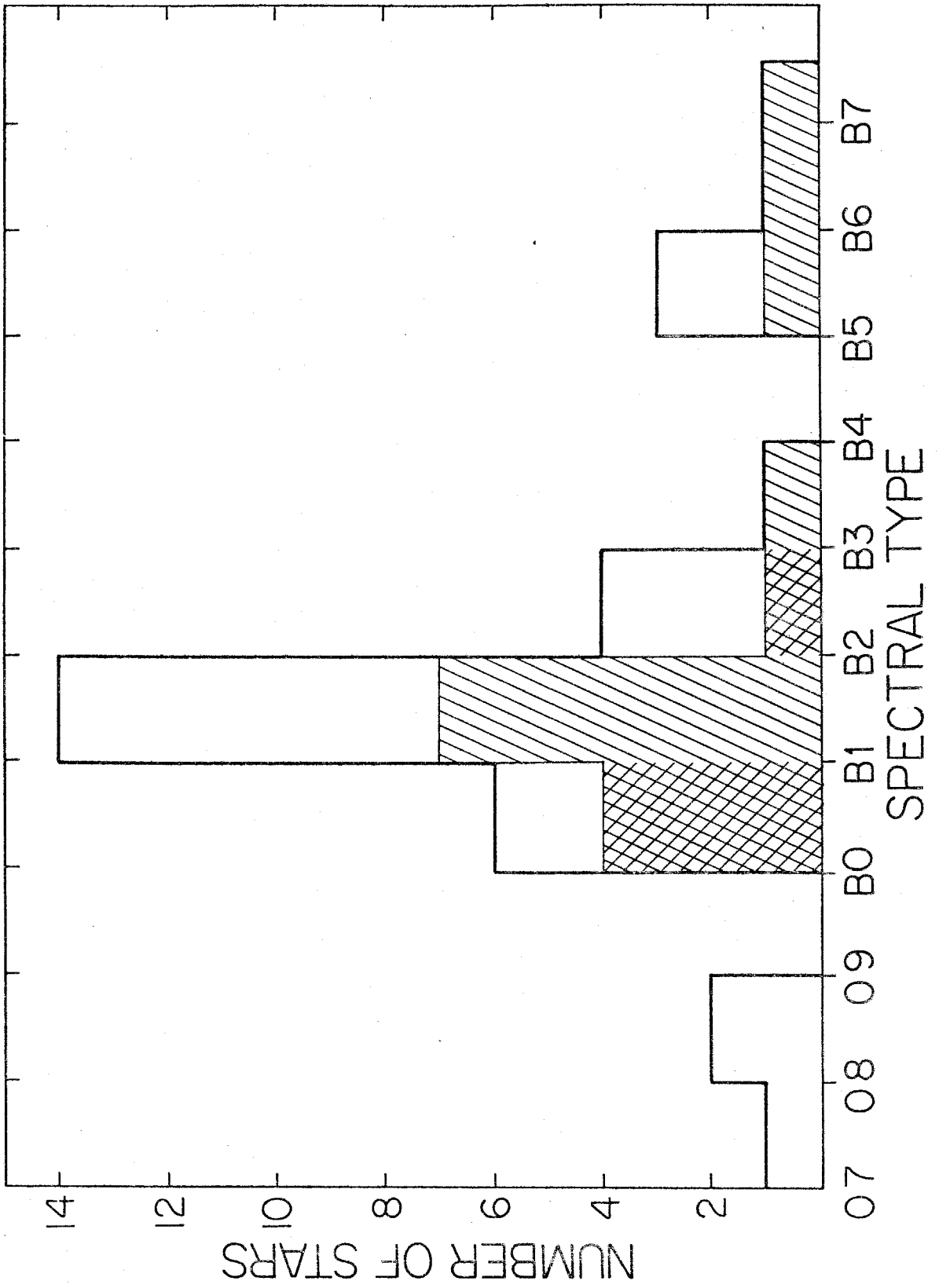


FIGURE 3b .

Distribution of interstellar extinctions among the Cepheus OB3 stars. Hatched regions indicate older subgroup members.

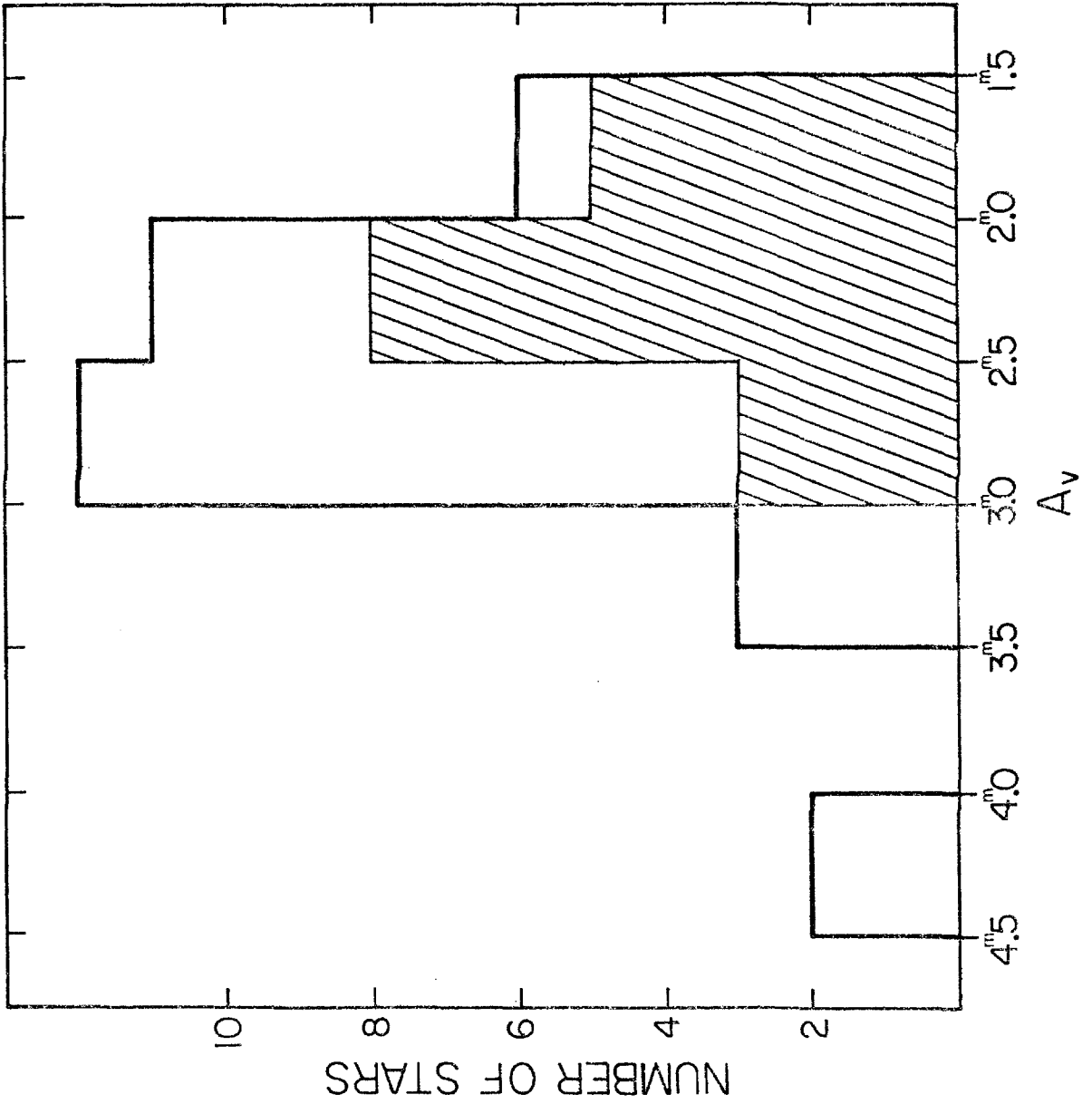


FIGURE 3c.

Distribution of radial velocities among the Cepheus
OB3 stars. Hatched regions indicate older subgroup members.

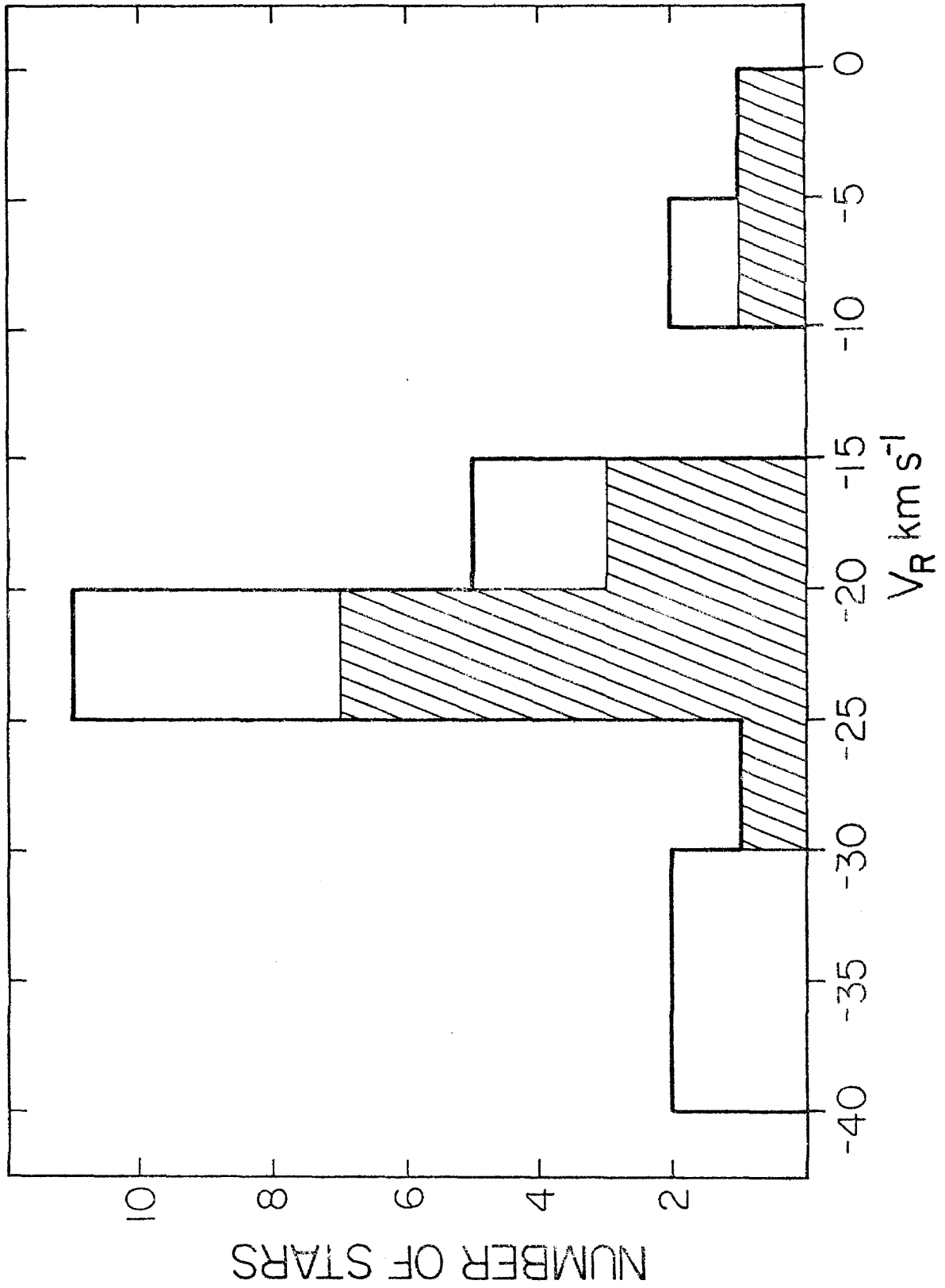


FIGURE 3d *

Distribution of proper motions in right ascension.

Hatched regions indicate older subgroup members.

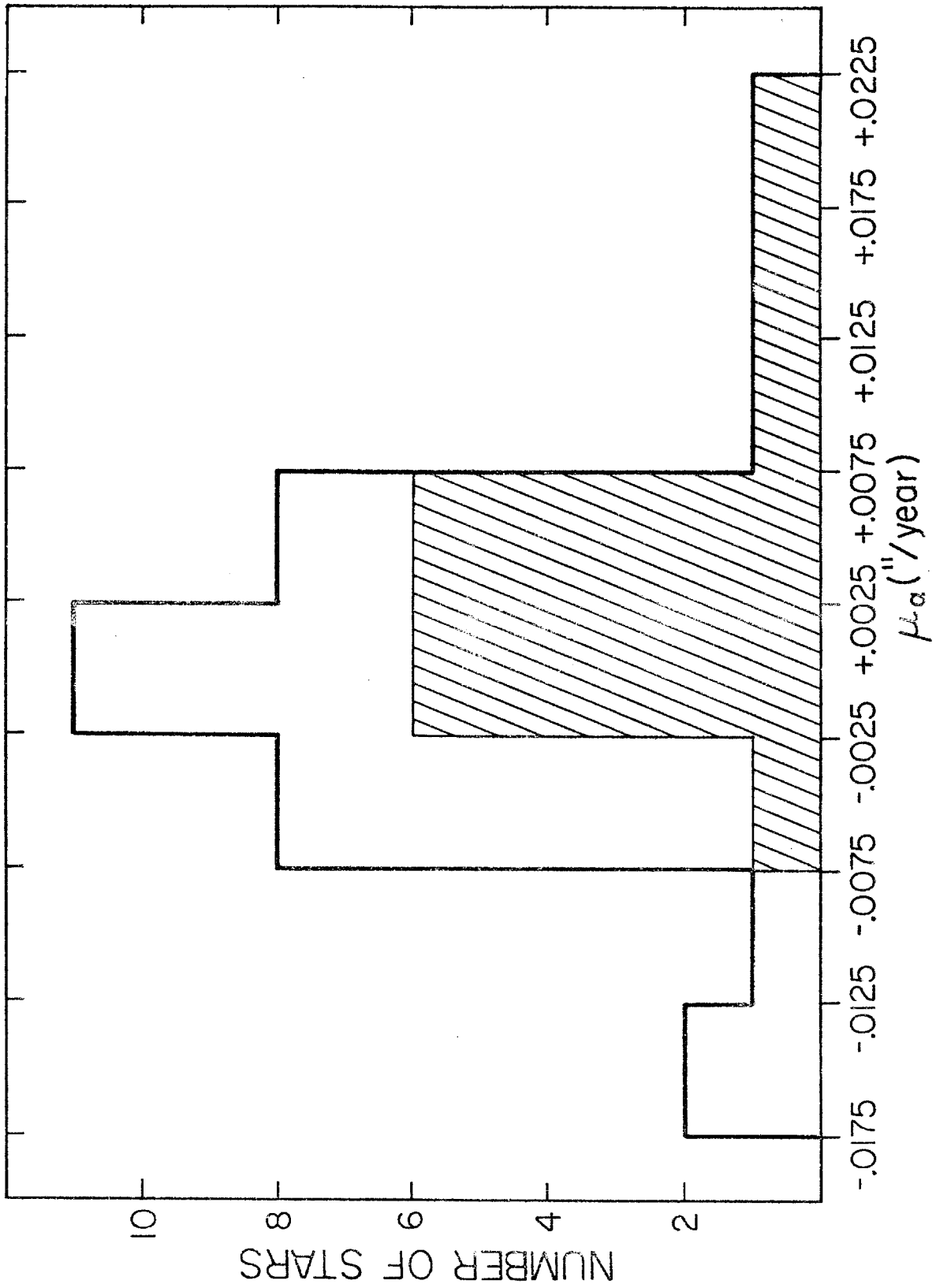
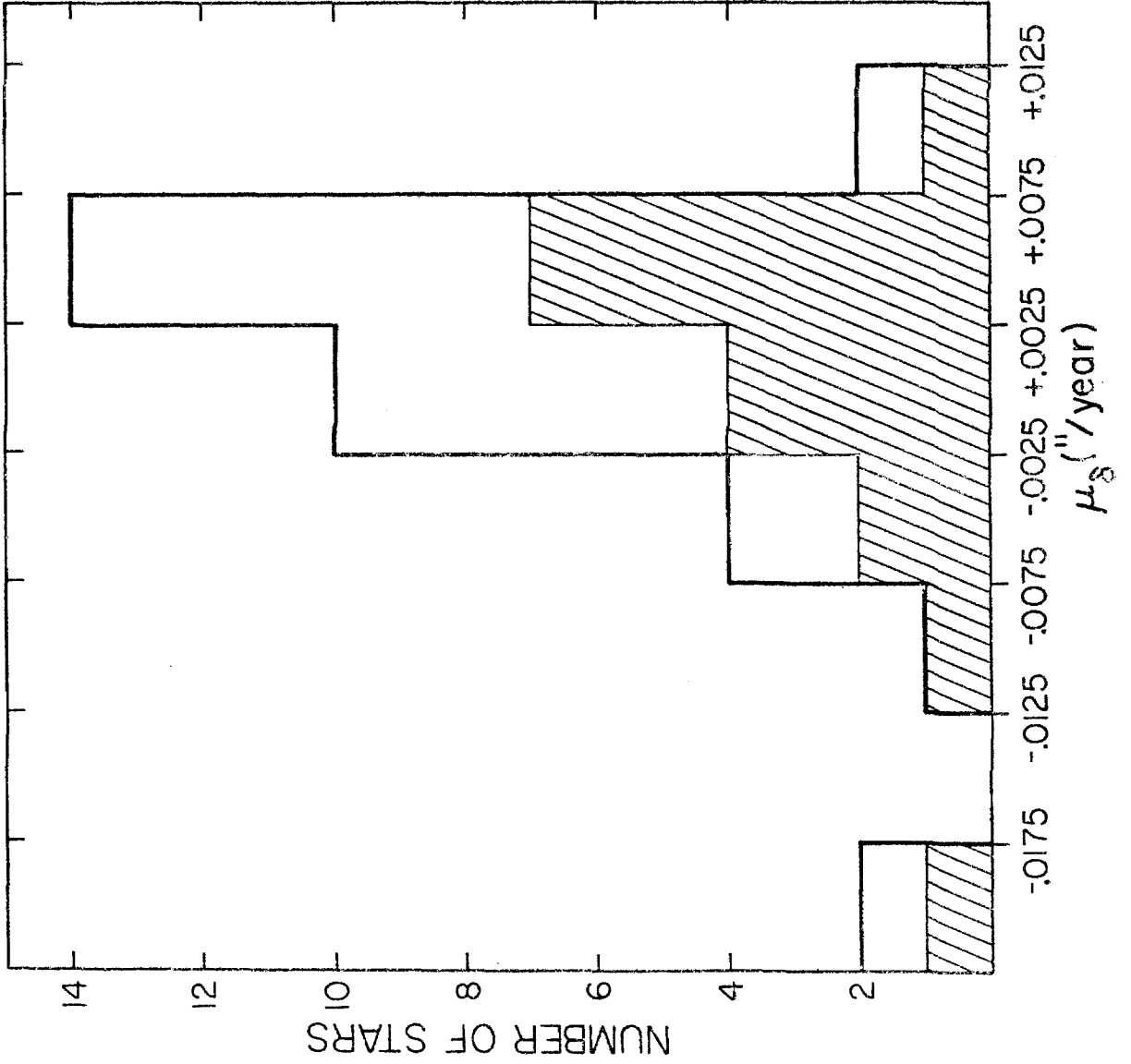


FIGURE 3e

Distribution of proper motions in declination.

Hatched regions indicate older subgroup members.



stars. While there is no clear-cut division of properties according to subgroup, there are tendencies for the older subgroup to have lower values of A_V , more positive radial velocities and more positive values of μ_α than the younger subgroup.

In the following discussions it will be important to bear in mind the fact that some stars cannot be unambiguously assigned to either subgroup. These stars and their properties are tabulated in Table 5 and may be compared with the distributions illustrated by Figure 3a through 3e. Their locations are evident from Figure 1. BHJ 44 and BHJ 59 are also included in Table 5. They are probably members of the older subgroup.

c) Pre-Main-Sequence Stars

The locations of any pre-main-sequence members of Cepheus OB3 are particularly important to a study of the way in which newly formed stars are related to the associated molecular cloud. Eggen (1976) has suggested that the peculiar spectra of BHJ 37 and BHJ 44 indicate that traces of their pre-main-sequence circumstellar shells still remain, implying that these stars have scarcely reached the main sequence, and are among the youngest association members. Their properties are given in Table 6. In Figure 1 they are represented by filled squares and their BHJ numbers are enclosed in parentheses.

TABLE 5
 PROPERTIES OF SELECTED STARS OF CEPHEUS OB3

BHJ	A_V (1)	Sp. Type (2)	V_R (3) (km s ⁻¹)	μ_α (3) (" / yr)	μ_δ (3) (" / yr)
25	1. ^m 99	B5	...	+0 ["] 0021	-0 ["] 0010
33	2. ^m 41	B5	...	-0 ["] 0005	-0 ["] 0063
39	2. ^m 26	B0.5	-18.3	-0 ["] 0061	-0 ["] 0065
37	2. ^m 1	B6Vnnp	...	+0 ["] 0104	+0 ["] 0050
44	1. ^m 9	B3V	-26.8
59	2. ^m 8	B2IV	...	+0 ["] 0064	+0 ["] 0017

(1) Blaauw et al. (1959)

(2) Garrison (1970)

(3) Garmany (1973)

TABLE 6

POSSIBLE PRE-MAIN-SEQUENCE STARS

BHJ	$V_O - M_V$	A_V	MK	V_R (km s^{-1})	" / yr μ_α	" / yr μ_δ
9	...	1.49	B7IV	-18.3	-0"0027	+0"0086
37	9.3	2.10	B6Vnp	...	+0"0104	+0"0050
42	...	2.14	+0"0159	+0"0046
44	...	1.90	B3V	-26.8
50	9.03	1.96	B3V	-18.0	+0"0072	-0"0115

Ultraviolet photometry of stars in the Cepheus region obtained by the ANS satellite indicates that several of these lie in regions of the color-magnitude diagram typically populated by pre-main-sequence stars (Kester 1977). In addition, Garmany (1973) has speculated that BHJ 9, BHJ 42 and BHJ 45, which lie somewhat to the right of the association main sequence and have proper motions comparable with those of the association stars, may be pre-main-sequence members. However, computations of distance moduli from the $ubvy$ and $H\beta$ photometry of Crawford and Barnes (1970), following the method of Eggen (1976 and references therein), immediately eliminate most of these stars from membership. An exception is BHJ 50. No $ubvy$ photometry and hence no accurate distance moduli are available for BHJ 9 and BHJ 42. Properties of these possible pre-main-sequence members of the association are also given in Table 6.

d) Subgroup Ages

In a recent proper-motion study Garmany (1973) has determined the expansion age of Cepheus OB3 to be 7.2×10^5 years. As already noted, this age corresponds to the time which has elapsed since the members of the association began to move away from their common origin. The state of evolution of the stars when expansion begins is not known. Some, or even all, may not have reached the main sequence. Thus, the expansion age gives an upper limit to the age of

the association provided that the onset of expansion occurs relatively quickly after the stars form, and that subsequent stellar motions are uniform. In Cepheus OB3 both these requirements appear to be fulfilled. There is no evidence of a bound core of O and B stars which would remain if expansion were due to dynamical relaxation of an established cluster (Gott 1973), nor is there any suggestion of retardation in the expansion velocity.

An upper limit to the association age can also be obtained from the upper main-sequence turnoff point. B_{HJ} 75, spectral type B0III, implies an age $\sim 10^7$ years (Iben 1964). However, this star may not be an association member and the expansion age, although uncertain because of proper-motion errors, will be accepted.

The upper limit to the association age is also the upper limit to the age of the older subgroup. A lower age limit may be established from the time required for the subgroup member of latest spectral type to contract to the main sequence. A B7V star, the latest type observed in the older subgroup, typically has a mass $\sim 5 M_{\odot}$ (Underhill 1966). Iben's (1965) pre-main-sequence contraction paths show that such a star will reach the main sequence after $\sim 5 \times 10^5$ years. It is concluded that the age of the older subgroup is $\sim 5-7 \times 10^5$ years.

Confirmation of this age estimate is provided by Garmany's (1973) proper-motion data. The expansion age

quoted above is derived from the expansion of the association as a whole. However, Garmany also noted some internal expansion in the older subgroup, from the motions in galactic latitude, and calculated an expansion age of 4.8×10^5 years. She found little evidence of internal expansion from motions in galactic longitude, but her data have been used here to determine an expansion age $\sim 10^6$ years. A weighted mean of these values gives an age of $\sim 7 \times 10^5$ years for the older subgroup.

It is difficult to determine an upper limit to the age of the younger subgroup since no main-sequence turnoff occurs among the stars. The latest spectral type observed is B5, but both stars of this type, BHJ 25 and BHJ 33, have been shown to be at least doubtful members of the subgroup. Their contraction time to the main sequence is estimated to be $\sim 3 \times 10^5$ years. If these stars are not members, the latest spectral type observed is B2.5. The corresponding main-sequence contraction time is $\sim 1 \times 10^5$ years. An age $\sim 1-3 \times 10^5$ years is deduced for the younger subgroup. Garmany's (1973) proper-motion data have been used again to obtain an approximate internal expansion age for this subgroup. From motions in galactic longitude, an age $\sim 3 \times 10^5$ years (some variation about this number results depending on which stars are accepted as subgroup members) is obtained, in good agreement with the age

suggested by the spectral types observed.

Blaauw (1964) assigned average ages of 8×10^6 years and 4×10^6 years respectively to the stars of the older and younger subgroups of Cepheus OB3 on the basis of their locations in the Hertzsprung-Russell diagram. The ages determined here are considerably lower, being $5-7 \times 10^5$ years and $1-3 \times 10^5$ years for the older and younger subgroups respectively. However, they are to be preferred to the earlier values since they derive from kinematic data and improved evolutionary time scales which were unavailable at the the time of Blaauw's initial studies of OB associations.

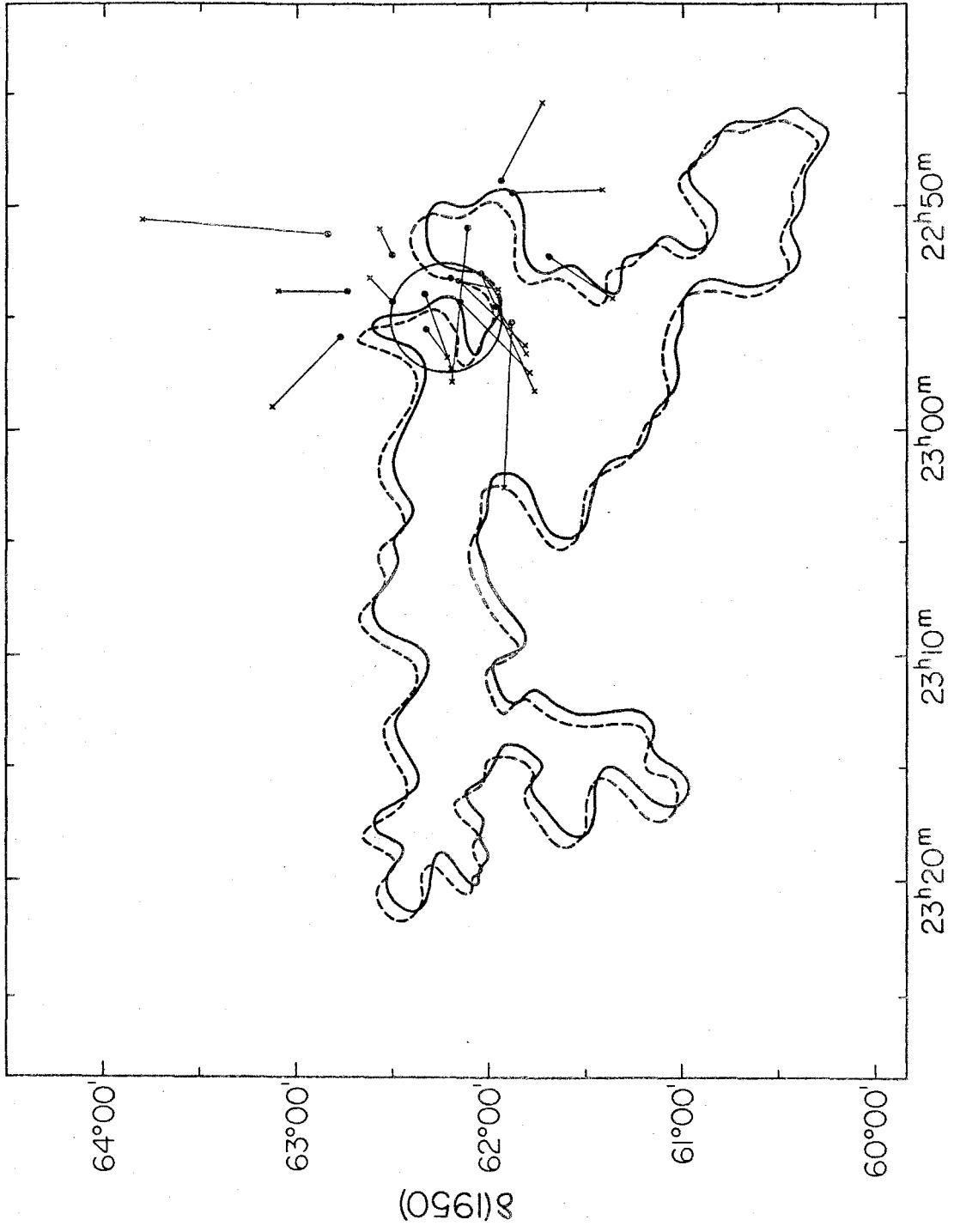
e) Origins of the Subgroups

The above subgroup ages were combined with Garmany's (1973) proper motions to establish where the subgroups formed.

Calculated positions for the younger subgroup stars 3×10^5 years ago and 1×10^5 years ago are shown in Figure 4a as crosses and filled circles respectively. Light solid lines connecting these symbols indicate trajectories in time. Solid lines outline the present boundary of the molecular cloud. Its location 10^5 years ago is derived by correcting only for the effects of differential galactic rotation and is described by dashed lines. Clearly the latter representation is purely schematic, since the

FIGURE 4a

Calculated positions for the younger subgroup members 1×10^5 years ago (filled circles) and 3×10^5 years ago (crosses). Light solid lines connecting the symbols represent time trajectories. The circle defines the area within which the younger subgroup was formed. The position of the cloud at present and 1×10^5 years ago is outlined by solid and dashed line respectively.



cloud may well have had a different form at that time.

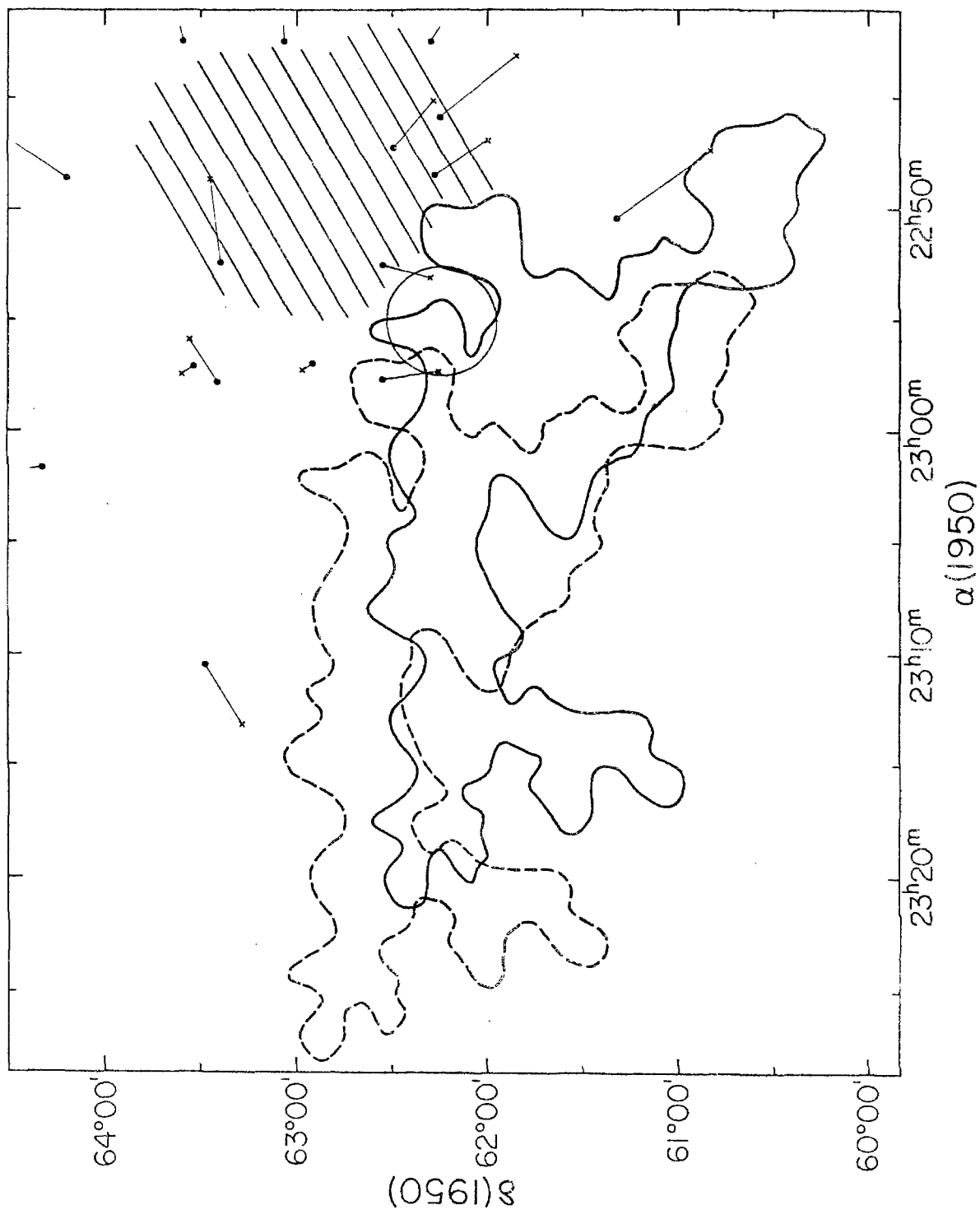
Because the errors inherent in the proper motions are large, no great weight can be placed on any individual stellar position. As a result, a "mean" position of origin for each subgroup was determined. A mean current position of the subgroup was derived by averaging the present positions of all members. This was then projected back in time, using the average of all proper motions for the subgroup. In the case of the younger subgroup the exclusion of doubtful members makes little difference to the final position. If the mean of all proper-motion errors within the subgroup is taken to be the error in this position, the light dotted circle in Figure 4a represents the area from which the younger subgroup could have originated within the derived time span.

A similar diagram for the older subgroup is shown in Figure 4b. The crosses and filled circles here result from ages of 7×10^5 and 5×10^5 years respectively, and the molecular cloud is schematically represented at its position 7×10^5 years ago. The possible area in which the stars of the older subgroup were born is shown as a lightly hatched region. This is considerably larger than its counterpart in Figure 4a mainly because of the longer time scale involved in the error determination.

A large fraction of the stars in the older subgroup

FIGURE 4b

Calculated positions for the older subgroup members 5×10^5 years ago (filled circles) and 7×10^5 years ago (crosses). The hatched area indicates the region within which the older subgroup formed. Light solid lines connecting the symbols represent time trajectories. The open squares show the present positions of Cep-A and Cep-C. The location of the cloud now and 7×10^5 years ago is represented by solid and dashed lines respectively.



have errors in proper motion comparable with the proper motions themselves. It is therefore not surprising that their calculated positions of origin fail to cluster in any way, unlike those of the younger subgroup. However, if it is conceded that these stars were born in the same region and are presently expanding away from each other, the area indicated in Figure 4b is not implausible. For comparison the supposed location of the younger subgroup at its time of formation is also drawn in Figure 4b. Although contiguous, the formation regions do not overlap, suggesting that the two subgroups formed in quite different locations.

IV. THE PRESENT RELATIONSHIP BETWEEN THE MOLECULAR CLOUD AND THE OB ASSOCIATION

Membership in the Cepheus OB3 association and in its individual subgroups, the ages and kinematics of the stars, and the structure and energetics of the related molecular cloud have been treated in some detail. The properties of the association and the cloud complex will now be summarized and the current relationship between the stars and the cloud will be considered.

Cepheus OB3 comprises two subgroups of ages $\sim 5-7 \times 10^5$ years and $\sim 1-3 \times 10^5$ years. Their separation on the plane of the sky is ~ 13 pc. The mean radial velocity, \bar{v}_{LSR} of the older subgroup is -9 km s^{-1} and that of the younger

subgroup -15 km s^{-1} (Garmany 1973). The proper motions (Garmany 1973) lead to mean tangential velocities, \bar{V}_T , equal $+19 \text{ km s}^{-1}$ and -14 km s^{-1} for the older and younger subgroups respectively. Most of the younger subgroup stars are seen in the direction of, or close to, the irregular H II region S155 (Sharpless 1959), for which $V_{\text{LSR}} = -15 \text{ km s}^{-1}$ (Miller 1968; Georgelin 1975). The exciting star or stars of this H II region have not been identified but they may be obscured by the Cepheus molecular cloud.

The mass of the molecular cloud is equal to a few thousand solar masses and its dimensions are $20 \text{ pc} \times 60 \text{ pc}$. In the cloud complex V_{LSR} ranges from -5 km s^{-1} to -15 km s^{-1} . The tangential velocity is unknown but, from the velocity of galactic rotation in this region, may be inferred to be $\sim 15 \text{ km s}^{-1}$. Within the cloud, and approximately 7 pc from the younger subgroup, is the region Cep-A of mass $\sim 500 M_{\odot}$, which appears to be collapsing to form a new subgroup of the association. Cep-B, where an embedded star may exist, lies close to and partially obscures the H II region S155. Both regions are located at the same end of the cloud as the birthplaces of the optically visible subgroups.

Blaauw (1964) has shown that in OB associations the younger subgroups appear on the plane of the sky to be more closely connected with the interstellar gas out of which

the stars presumably formed, while progressively less gas is seen in association with older subgroups. This is certainly the case in Cepheus OB3 and it therefore seems logical to presume that the advance of star formation may be followed across the association, through the successively younger groups of stars and into the cloud itself, where, as described above, there are signs that stars are currently being made. It seems likely that optically visible pre-main-sequence stars will be situated closest to the molecular cloud and will give some indication of the pattern of star formation.

Possible pre-main-sequence members of the association are listed in Table 5. Spectral classification of BHI 15 (see Table 5) and the fact that it illuminates a reflection nebula (BHI 15 \equiv +62°2361 \equiv vdB 155, van den Bergh 1966), suggests that this is also a recently formed member of the younger subgroup. These stars are not found preferentially closer to the molecular cloud (see Fig. 1). It appears that when expansion of the association begins, not all of its members have reached the main sequence, and at the present time there are, in both subgroups, stars still in the contraction phase. Thus, the positions of the subgroups as a whole, rather than the current locations of individual pre-main-sequence or very young stars, are important in establishing the progression of star formation through the

association.

It also seems most probable that if remnants of the primeval cloud still exist these will be found preferentially around the youngest members. However, the searches for CO in the directions of the association stars described in Chapter 1, resulted in detections only for the stars in Table 7. Parentheses indicate very uncertain measures. The only possible pre-main-sequence star among these is BHJ 42 and since its velocity is unknown it is impossible to determine its position in the line of sight relative to the molecular cloud. Among the very young association stars CO is observed only toward BHJ 15. In this instance and also for the relatively young BHJ 16, the velocities of CO emission are so very different from the stellar velocities that stars and gas do not appear to be physically related.

For the remaining stars in Table 7 there is no obvious relation between age as indicated by spectral classification and CO intensity. Where stellar velocities exist, they are in good agreement with the gas velocities, implying that the stars lie within the cloud. The strongest CO emission is seen in the direction of stars having the greatest values of absolute visual extinction, as might be expected from the roughly linear correlation which obtains between gas column density and A_v (Dickman 1976 and references therein).

TABLE 7

CO DETECTION IN THE DIRECTION OF STARS

BHJ	MK ^c	V_{CO} (km s ⁻¹)	V_* (km s ⁻¹)	T_{A}^* (K)	A_{V}^a	
11	BIV	-11	-13	4.4	4. ^m 26	(1)
15	B2IV-Vne	- 9	-29	4.9	2. ^m 89	(1)
16	B0.5V	-10	-22	4.0	2. ^m 91	(1)
17	B1.5V	-11 ^b	...	2.9	3. ^m 18	(1)
24	BIV	[-12]	-12	[~1]	3. ^m 01	(1)
42	...	-15	...	[3]	2. ^m 14	(3)
56	BIV	[-14]	-14	2.3	2. ^m 35	(2)
75	B0III	[-15]	-13	[1.5]	2. ^m 64	(2)

(1) Younger subgroup member

(2) Older subgroup member

(3) Possible pre-main-sequence star

a Calculated after Blaauw *et al.* (1959)

b Note difference in velocity from BHJ 17 - 8S4E
(Table 1, Chapter 1)

c Garrison (1970)

There is no evidence of the enhanced density expected in a remnant of the primeval cloud around a newly formed star. Emission intensities in these directions reflect only the conditions within the cloud lying in front of the stars in the line of sight. This is true even for BHJ 56 where CO is observed at a considerable distance from the primary cloud. It seems most probable that in this case the juxtaposition of an association star and the gas occurs by chance.

Some deviation from this general pattern is noticed around BHJ 11 where, over a very limited area (~ 0.5 pc x 0.5 pc), CO emission is enhanced above the values typically observed in that region of the cloud. Emission from both isotopic species is usually detected at velocities of the order of -8 or -9 km s⁻¹, the ¹³CO being weak, as the ¹²CO measures would imply (see Chapter 1). The ¹²CO emission becomes noticeably stronger close to BHJ 11, but its velocity varies with position, being ~ -11 km s⁻¹ at the stellar position and becoming less negative (and closer to the average cloud velocity) at increasing distance from the star. The -11 km s⁻¹ feature appears to be a blend of -13 km s⁻¹ (the stellar velocity) and -9 km s⁻¹ (the cloud velocity) lines. There is no corresponding variation in the ¹³CO velocity. It is presumed that BHJ 11 has moved some distance from its place of origin and is now responsible for purely local heating of the cloud.

The evidence suggests that with the exception of BHJ 11 there is currently little interaction between the association stars and the molecular cloud. It is indeed questionable if BHJ 11 is an association member (see § IIIa).

V. STAR FORMATION IN CEPHEUS OB3

It remains to ascertain how the present Cepheus OB3 complex was produced. Recently Elmegreen and Lada (1977b) have presented a theory of how star formation, once initiated, proceeds in OB associations. A unique process for creating the initial subgroup has not yet been identified, although a number of mechanisms have been suggested. These include cloud-cloud collisions (Loren 1976), partial cloud collapse induced by the passage of the galactic density wave (Mouschovias, Shu and Woodward 1974; Woodward 1976), and supernova explosions (Berkhuijsen 1974; Sancisi 1974; Assousa et al. 1977; Herbst and Assousa 1977). Following a suggestion by Öpik (1953), Ögelman and Märan (1976) have indeed proposed that not only the first, but also all following bursts of star formation in OB associations are caused by supernovae. Cepheus OB3 will now be examined to determine which star forming process or processes are applicable.

Star formation is taking place at only one edge of the

molecular cloud. Various stages are identified schematically in Figure 4b; in the hatched area the older subgroup was born $5-7 \times 10^5$ years ago; immediately between this and the cloud itself the younger stars were created $1-3 \times 10^5$ years ago in the area described by a circle; continuing into the cloud itself, a newly formed star may be currently embedded in Cep-B; a new subgroup, denoted by an open square, is apparently forming at Cep-A; and Cep-C, also denoted by an open square, may be the precursor of a region such as Cep-A.

At the present time there is a striking absence of gas in the environs of the older subgroup, but some younger subgroup stars are found near to, or within, the cloud (see § IV). On the Palomar Sky Survey prints a few younger subgroup members appear against the extended H II region, S155. These stars have values of V_{LSR} very close to that of S155, and apparently lie within the H II region.

The mean radial velocities of the subgroups, -9 km s^{-1} for the older and -15 km s^{-1} for the younger, are comparable to the range of velocities observed in the Cepheus OB3 cloud complex. However, the mean tangential velocity of the older subgroup, $+19 \text{ km s}^{-1}$, is oppositely directed to that of the younger subgroup, -14 km s^{-1} , and the molecular cloud, $\sim -15 \text{ km s}^{-1}$. Uncertainties in the radial velocities are of order $\pm 5 \text{ km s}^{-1}$. The proper motions give rise to uncertainties of at least 50% in the tangential velocities,

but the older subgroup appears to be moving away from the primeval cloud with a velocity of $34 \pm 9 \text{ km s}^{-1}$. Any theory of how stars are created in Cepheus OB3 must explain both the absence of gas around the older subgroup stars and the widely differing tangential velocities of the subgroups.

These velocities in fact suggest that since their formation, the older subgroup stars have merely separated from the cloud. Taking for the cloud $V_T = -15 \text{ km s}^{-1}$ and extrapolating forwards in time by $5-7 \times 10^5$ years, it is found that by now the primeval cloud of the older subgroup (represented schematically by the hatched area of Fig. 4b) should lie within a region bound by $22^{\text{h}}38^{\text{m}}$ and $22^{\text{h}}50^{\text{m}}$ in right ascension and by $61^{\circ}30'$ and $63^{\circ}30'$ in declination. Inspection of the Palomar Sky Survey prints shows some obscuration in the southern part of this region which may be a remnant of the molecular cloud out of which the subgroup formed. The CO observations do not extend sufficiently far west for its structure to have been examined.

A considerable number of molecular clouds, apparently connected with OB associations, have now been detected. Their masses and dimensions are generally very similar, but are somewhat larger than those of the Cepheus cloud (Blitz 1977). An increase of 20 pc in the longitudinal dimensions of the Cepheus OB3 cloud would not only bring its size and mass closer to that of other association clouds, but would

also encompass the obscured region mentioned above. It seems plausible that the parent cloud was more extensive than the present observations imply. A superficial comparison of the obscuration in this unobserved region with that in the area of the known cloud does, however, indicate that the extension is fragmentary in nature.

In explanation of the absence of CO in galactic clusters with main-sequence turnoffs at spectral types later than B0 (Bash, Green and Peters 1977), Wheeler and Bash (1977) have shown that a supernova of $\sim 20 M_{\odot}$ (the mass of a very early B or late O star) can effectively break up a $10^4 M_{\odot}$ molecular cloud. In Cepheus OB3 no stars later than B0 are evolving away from the main sequence and, according to their hypothesis, CO should still be present since no member star should have evolved to the point of exploding and disrupting the remaining cloud. While CO is not presently detected among the members of the older subgroup, it appears to be present at positions where they would be expected had they not possessed such large velocities. The present observations therefore do not contradict the conclusions of Bash and Wheeler.

The disparity between older subgroup velocities and those of the younger subgroup and the molecular cloud indicate that the formation mechanisms for the subgroups are probably quite different. Some event capable of

endowing the older subgroup with such velocities must have occurred at the time of their formation. One possibility is a supernova explosion, which would affect the velocity of the gas from which the star formed.

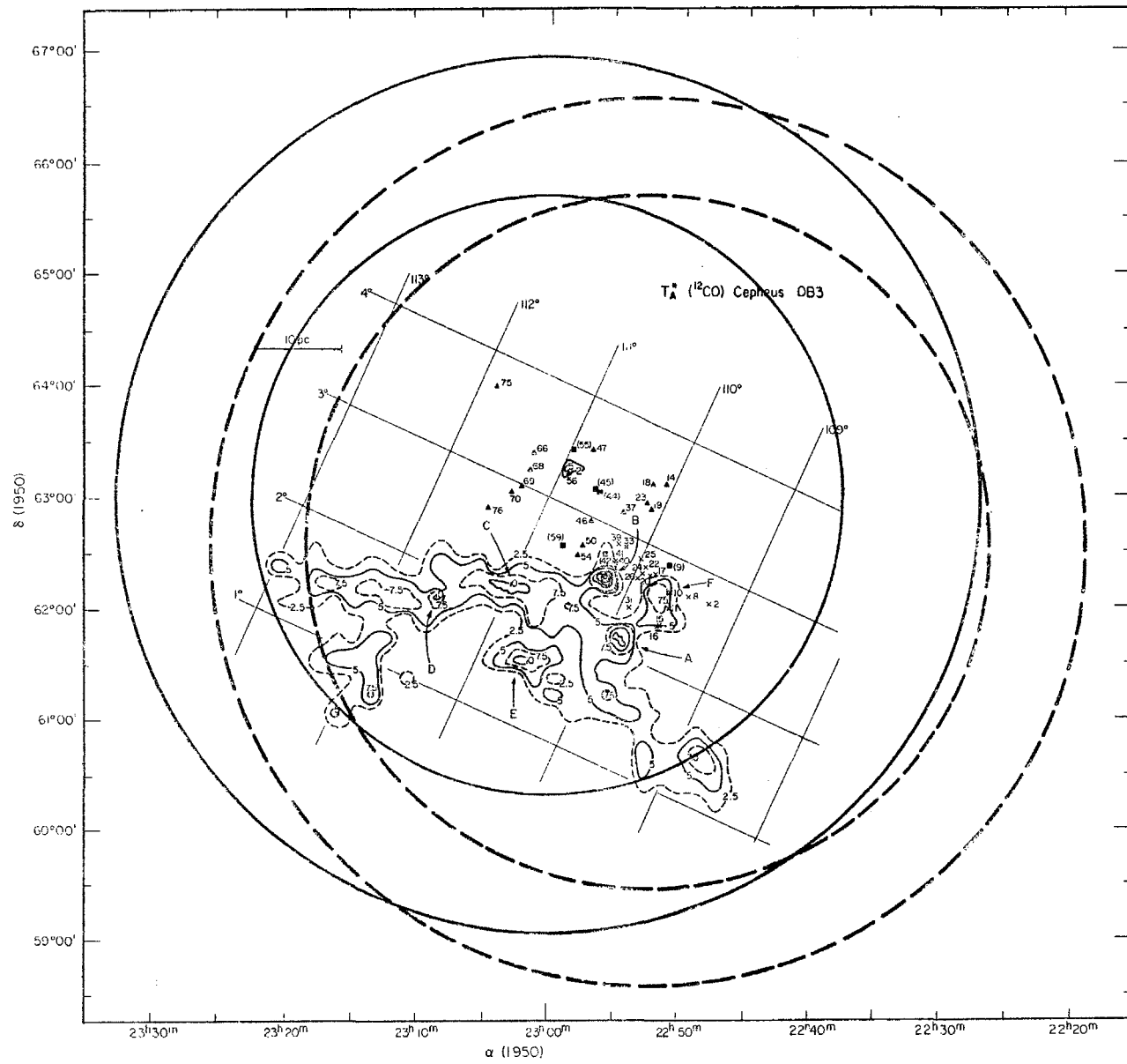
There is some evidence for the presence of a supernova remnant around Cepheus OB3. In their 21-cm line survey of the region, Simonson and van Someren Greve (1975) detected an H I shell of mass $5 \times 10^4 M_{\odot}$ and radius 4° , centered on $l = 110^{\circ}$, $b = 3^{\circ}$ and expanding at 10 km s^{-1} . More recently, Assousa et al. (1977) using the data of Weaver and Williams (1974) have confirmed the existence of a shell but contend that it is centered at $l = 111^{\circ}$, $b = 3^{\circ}$, and has an expansion velocity of 35 km s^{-1} . The locations of these shells with respect to the association and the cloud complex are shown schematically in Figure 5.

Assousa et al. (1977) derive an age of 4.5×10^5 years for the remnant. The data of Simonson and van Someren Greve (1975) lead to an age of 1.6×10^6 years. Within the errors, either age is compatible with the hypothesis that the supernova explosion initiated the formation of the older subgroup. However, it is difficult to reconcile the present velocity of the stars with a current shell velocity of 35 km s^{-1} . The present location of the stars with respect to the shell is also somewhat surprising.

Since the ages are so large it is unlikely that the

FIGURE 5

Schematic representation of the present position of the supernova shell on the plane of the sky. The solid lines indicate the shell centered on $\ell = 111^\circ$, $b = 3^\circ$ (Assouza et al. 1977), and the dashed lines the shell centered on $\ell = 110^\circ$, $b = 3^\circ$ (Simonson and van Someren Greve 1975).



identification of the hydrogen shell as a supernova remnant can be confirmed by the detection of non-thermal radio continuum radiation. However, Assoua et al. (1977) point out that the pulsar PSR 2223+65 at $l = 108.6^\circ$, $b = 6.9^\circ$, at 730 pc and of age 1.4×10^6 years (Taylor and Manchester 1975), may well be a result of the original supernova explosion. A tangential velocity of $\sim 53 \text{ km s}^{-1}$ (0.0154 arcseconds per year), which is somewhat low for a pulsar, would be required to traverse the distance between the supernova center and the present position in the given time scale. Unfortunately, proper motions are not known for this object. There appears to be no conclusive evidence that star formation in Cepheus OB3 was triggered by a supernova explosion.

There remains the possibility that the Cepheus OB3 association formed as a result of the passage of the galactic density wave. The older subgroup has a peculiar velocity with respect to the cloud only in the tangential direction, implying that the stars were formed as a result of compression of interstellar matter by a shock front moving in the opposite direction to that of galactic rotation. At the position of Cepheus OB3 the velocity of galactic rotation is greater than the pattern speed of the galactic density wave (Roberts 1969), so that gas passes through the shock in such a way that any stars formed will

preferentially move in the sense opposite to galactic rotation. However, the association lies in the Orion spur which may be a material arm, and in this situation high velocities are not easily explained.

Although the way in which star formation is initiated remains uncertain, it seems plausible that the sequential formation mechanism proposed by Elmegreen and Lada (1977b) applies in Cepheus OB3. It appears that the younger subgroup, created in the compressed region between the ionization front produced by the older subgroup stars and its related shock front, has now emerged from this compressed region and is ionizing the surrounding gas. A new compressed layer is indicated by Cep-A and possibly Cep-C.

Unfortunately, while the general pattern observed in Cepheus OB3 agrees with the theory of Elmegreen and Lada, the details do not. They find typical time scales between bursts of star formation of $\sim 2-3 \times 10^6$ years, and corresponding distances of 10-20 pc. This distance is in reasonable agreement with the observations in this association, but the time is much too high. The difference in age between the subgroups has been shown to be $\sim 4 \times 10^5$ years. A collapse time of $\sim 3 \times 10^5$ years for Cep-A gives an age difference between it and the younger subgroup which is also $\sim 5 \times 10^5$ years. Elmegreen and Lada admit that density inhomogeneities in the cloud can

modify their model considerably and suggest that within the compressed layer stars may form first from fragments which initially had higher densities than their surroundings. (In the Cepheus cloud the layer could conceivably extend from Cep-C to Cep-A, the unstable regions reflecting higher density areas of the original cloud.) Assuming their variable N_0 (the number of main-sequence O stars per 10 pc^2 in an OB subgroup) to be constant, the time between bursts of star formation, t_I , scales as $n^{-1/2}$, where n is the hydrogen density in the cloud; the distance between the formation zones, r_I , scales as $n^{-4/5}$. There is thus no way in which t_I can be reduced without significantly affecting the acceptable values of r_I .

The projected formation time of the new subgroup was determined assuming Cep-A to be in free-fall collapse. Elmegreen and Lada point out that their t_I is in fact larger than the growth time of a Jeans instability in the molecular cloud and that this may be an impediment to their model. They contend, that observational evidence indicates that free fall of the cloud as a whole does not occur. The observations presented here agree with this argument. However, individual fragments of the cloud can be in free-fall collapse, and in Cepheus OB3 the difference in ages between the known subgroups is comparable to the free-fall collapse times of these fragments.

VI. SUMMARY

Observations of the Cepheus OB3 molecular cloud and of the association stars have been extensively analyzed. The suggestion of Chapter 1 that Cep-A and Cep-C are regions of enhanced density have been confirmed, and it has been established that a new subgroup of the association may be forming in Cep-A on a time scale of $\sim 3 \times 10^5$ years. There is sufficient mass available in this fragment to give rise only to the usual number of O and B stars found in an OB subgroup. It appears that lower mass stars must form elsewhere, possibly as a result of fragmentation and collapse of much smaller portions of the cloud. There is some evidence that an embedded star may be present in Cep-B.

Ages of the individual subgroups, and a formation time for that currently being created in Cep-A, have been determined. It is suggested that the subgroups may be considerably younger than the ages originally given by Blaauw. Their ages are $5-7 \times 10^5$ years and $1-3 \times 10^5$ years.

Star formation appears to begin at one end of, and then proceed sequentially through, the molecular cloud. Available calculations of such a process do not apply in detail to the Cepheus OB3 association, principally because of the revised subgroup ages.

The way in which star formation is initiated remain

uncertain. While it seems unlikely that supernovae are always the authors of star formation in OB associations, that they occasionally are is supported by observations of Per OB2, Sco OB2 and Lac OB1 (Sancisi 1974; Sancisi et al. 1974), and the possibility that the older subgroup of Cepheus OB3 formed in a supernova shell cannot be entirely ruled out. A test of the more general applicability of the supernova hypothesis, which would also take into account the likelihood of density wave related star formation, might be made by examining the relative positions and velocities of the stars and gas in the associations Cep OB2 and Cep OB4. These are at about the same distance as Cep OB3 but on either side of it in the Orion arm.

The disparity between the tangential velocities of the older subgroup and those of the cloud and the younger subgroup in fact suggests that the method by which star formation is initiated is very different from the way in which it propagates in Cepheus OB3. Whether this is a property common to OB associations or whether it holds only in this case is a subject for further study.

REFERENCES

- Assousa, G. E., Herbst, W., and Turner, K. C. 1977, pre-print.
- Bash, F. N., Green, E. M., and Peters, W. L. 1977, Ap. J., in press.
- Berkhuijsen, E. M. 1974, Astr. Ap., 35, 429.
- Blair, G. N. 1976, Ph.D. thesis, University of Texas at Austin.
- Blair, G. N., Evans, N. J., Vanden Bout, P. A., and Peters, W. L. 1977, Ap. J., in press.
- Blaauw, A. 1958, A. J., 63, 186.
- _____. 1964, Ann. Rev. Astr. Ap., 2, 213.
- Blaauw, A., Hiltner, W. A., and Johnson, H. L. 1959, Ap. J., 130, 69.
- Blitz, L. 1977, private communication.
- Conti, P. S., and Burnichon, M. L. 1975, Astr. Ap., 38, 467.
- Crawford, D. L., and Barnes, J. V. 1970, A. J., 75, 952.
- Cruz-Gonzales, C., Recillas-Cruz, R., Costero, R., Peimbert, M., and Torres-Peimbert, S. 1974, Rev. Mexicana Astr. Astrof., 1, 211.
- Dickman, R. L. 1976, Ph.D. thesis, Columbia University.
- Elmegreen, B. G., and Lada, C. J. 1977a, A. J., 81, 1089.
- _____. 1977b. Ap. J., 214, 725.
- Eggen, O. J. 1976, Q.J.R.A.S., 17, 472.

- Encrenaz, P. J., Falgarone, E., and Lucas, R. 1975,
Astr. Ap., 44, 73.
- Evans, N. J., Blair, G. N., and Beckwith, S. 1977,
Ap. J., in press.
- Evans, N. J., and Kutner, M. L. 1976, Ap. J. (Letters),
204, L131.
- Garmany, C. 1973, A. J., 78, 185.
- Garrison, R. F. 1970, A. J., 75, 1001.
- Georgelin, Y. M. 1975, Ph.D. thesis, Universit e de
Provence, Observatoire de Marseilles.
- Goldreich, P., and Kwan, J. 1974, Ap. J., 189, 441.
- Gott, J. R. 1973, Ap. J., 186, 481.
- Harris, D. L., Strand, K. Aa., and Worley, C. E. 1963,
Basic Astronomical Data, ed. K. Aa. Strand (Chicago:
University of Chicago Press), p. 273.
- Herbst, W., and Assousa, G. E. 1977, Ap. J., in press.
- Hollenbach, D. J., Werner, M. W., and Salpeter, E. E.
1971, Ap. J., 163, 165.
- Iben, I. 1964, Ap. J., 139, 1631.
_____. 1965, Ap. J., 141, 993.
- Jenkins, E. B., and Savage, B. D. 1974, Ap. J., 187, 243.
- Kester, D. 1977, private communication.
- Knapp, G. R., Kuiper, T. B. H., Knapp, S. L., and
Brown, R. L. 1976, Ap. J., 206, 443.
- Kutner, M. L., and Tucker, K. 1975, Ap. J., 199, 79.

- Leung, C. M., and Brown, R. L. 1977, Ap. J. (Letters),
214, L73.
- Loren, R. B. 1976, Ap. J., 209, 466.
- Loren, R. B., Peters, W. L., and Vanden Bout, P. A.
1974, Ap. J. (Letters), 194, L103.
- Lovas, F. J., and Tiemann, E. 1974, J. Chem. Ref. Data,
3, 609.
- Miller, J. S. 1968, Ap. J., 151, 473.
- Mouschovias, T. Ch., Shu, F. H., and Woodward, P. R.
1974, Astr. Ap., 33, 73.
- Ögelman, H. B., and Maran, S. P. 1976, Ap. J., 209, 124.
- Öpik, E. J. 1953, Irish Astr. J., 2, 219.
- Panagia, N. 1973, A. J., 78, 929.
- Penzias, A. A., Jefferts, K. B., and Wilson, R. W.
1971, Ap. J., 165, 229.
- Prentice, A. J. R., and Ter Haar, D. 1969, M.N.R.A.S.,
146, 423.
- Roberts, W. W. 1969, Ap. J., 158, 123.
- Sancisi, R. 1974, IAU Symposium No. 60, Galactic Radio
Astronomy, ed. F. J. Kerr and S. C. Simonson (Boston:
D. Reidel Pub. Co.), p. 115.
- Sancisi, R., Goss, W. M., Andersson, C., Johansson, B.,
and Winnberg, A. 1974, Astr. Ap., 35, 445.
- Scalo, J. M. 1977, Ap. J., 213, 705.
- Scoville, N. Z., and Kwan, J. 1976, Ap. J., 206, 718.

- Scoville, N. Z., Solomon, P. M., and Penzias, A. A. 1975, Ap. J., 201, 352.
- Sharpless, S. 1959, Ap. J. Suppl., 4, 257.
- Simonson, S. C., and van Someren Greve, H. W. 1975, Astr. Ap., 49, 343.
- Snell, R. L., and Loren, R. B. 1977, Ap. J., 211, 122.
- Spitzer, L. 1968, Diffuse Matter in Space (New York: Interscience).
- Taylor, J. H., and Manchester, R. N. 1975, A. J., 80, 794.
- Torres-Peimbert, S., Lazcano-Aranjo, A., and Peimbert, M. 1974, Ap. J., 191, 401.
- Underhill, A. B. 1966, The Early Type Stars (Dordrecht-Holland: D. Reidel Pub. Co.).
- van den Bergh, S. 1966, A. J., 71, 990.
- Weaver, H., and Williams, D. R. W. 1974, Astr. Ap. Suppl., 17, 1.
- Wheeler, J. C., and Bash, F. N. 1977, Nature, 268, 706.
- Woodward, P. 1976, Ap. J., 207, 484.
- Wootten, H. A., Snell, R. L., Blair, G. N., Evans, N. J., and Vanden Bout, P. A. 1977, preprint.